Review Article

ADVANCED PHOTONICS

Organic near-infrared optoelectronic materials and devices: an overview

Zong-Lu Che,[a,†] Chang-Cun Yan,[a,b,*,†] Xue-Dong Wang,[a,*] and Liang-Sheng Liao[a,c,*]

[a]Soochow University, Institute of Functional Nano and Soft Materials (FUNSOM), Jiangsu Key Laboratory for Carbon-Based Functional Materials and Devices, Suzhou, China

[b]Soochow University, College of Chemistry, Chemical Engineering and Materials Science, Jiangsu Engineering Laboratory of Novel Functional Polymeric Materials, Suzhou, China

[c]Macau University of Science and Technology, Macao Institute of Materials Science and Engineering, Macau, China

Abstract. Near-infrared (NIR) light has shown great potential for military and civilian applications owing to its advantages in the composition of sunlight, invisibility to human eyes, deeper penetration into biological tissues, and low optical loss in optical fibers. Therefore, organic optoelectronic materials that can absorb or emit NIR light have aroused great scientific interest in basic science and practical applications. Based on these NIR organic optoelectronic materials, NIR optoelectronic devices have been greatly improved in performance and application. In this review, the representative NIR organic optoelectronic materials used in organic solar cells, organic photodetectors, organic light-emitting diodes, organic lasers, and organic optical waveguide devices are briefly introduced, and the potential applications of each kind of device are briefly summarized. Finally, we summarize and take up the development of NIR organic optoelectronic materials and devices.

Keywords: near-infrared; organic optoelectronic materials; organic solar cells; organic light-emitting devices; organic optical waveguides.

Received Feb. 28, 2023; revised manuscript received Oct. 8, 2023; accepted for publication Dec. 6, 2023; published online Jan. 8, 2024.

[DOI: 10.1117/1.AP.6.1.014001]

1 Introduction

Near-infrared (NIR) light is an electromagnetic wave whose wavelength is in the range of 780 to 2500 nm, between visible light and mid-infrared light.[1,2] Compared with visible light and ultraviolet (UV) light with shorter wavelengths, NIR light has several advantages, such as invisibility to the human eye, strong penetration in biological tissues, and low optical loss in optical fibers.[3,4] Based on these advantages, NIR light has been widely used in the medical, industrial, military, energy, and other fields.[5] In addition, NIR light is the main component of sunlight. In the spectrum of sunlight, NIR light (780 to 2500 nm) accounts for 52% of total energy, which is higher than that of visible light (43%).[5,6] Hence, the advancement of NIR optoelectronic materials capable of absorbing or emitting NIR light holds significant importance. According to the composition, NIR optoelectronic materials can be split into two categories: inorganic optoelectronic materials and organic optoelectronic materials. Compared with inorganic materials, organic NIR optoelectronic materials have the advantages of inherent biocompatibility, mechanical flexibility, and solution processability. Moreover, organic materials are characterized by diverse structures and easily tunable properties.[7–9] Based on these properties, organic NIR optoelectronic materials have attracted great attention and been widely used in organic solar cells (OSCs), organic photodetectors (OPDs), organic light-emitting diodes (OLEDs), organic lasers, and organic light waveguides.[5,10–13]

According to different mechanisms of action, organic NIR optoelectronic materials can be divided into two categories: organic NIR-absorbing materials that can absorb NIR light and convert it into electrical signals, and organic NIR-emitting materials that can emit NIR light when stimulated by photoexcitation, an electric field, or a chemical reaction. Organic NIR-absorbing materials are important working materials in

*Address all correspondence to Chang-Cun Yan, cyan@suda.edu.cn; Xue-Dong Wang, wangxuedong@suda.edu.cn; Liang-Sheng Liao, lsliao@suda.edu.cn

†These authors contributed equally to this work.

OSCs and OPDs.[14–16] For example, OSCs based on organic NIR-absorbing materials can extend their absorption range into the NIR region, which can make full use of sunlight and thereby enhance their power conversion efficiency (PCE) effectively.[3,11] Among OPDs, the invisible detecting light with less interference endows them with great potential in industrial, military, and scientific applications.[17–19] For NIR absorption materials, the most crucial aspect is to increase the generation of photoexcited charge carriers within the material. For NIR organic materials, the construction of donor (D)–acceptor (A) structures is usually used to increase their photogeneration charge carrier.[20] The mechanism is shown in Fig. 1(a), where the donor or acceptor absorbs photons and generates excitons to diffuse to the interface. At this point, the excitons dissociate to generate free electrons and holes and are transported by polariton hopping, thus forming an electrical signal.[21]

Organic NIR-emitting materials have a significant role and research value in OLEDs because of their invisibility to the naked eye, high penetration, low background interference, and lack of harm to living organisms.[22,23] In addition, organic NIR emitting materials have important applications in the field of NIR organic lasers due to their intrinsic four-level energy system[24] and large excited emission cross section.[25] Moreover, the three communication windows with low loss in optical fiber communication are 850 nm (first window), 1310 nm (second window), and 1550 nm (third window), which are all located in the NIR region, thus making organic NIR-emitting materials have great potential for applications in optical waveguides.[26–28] According to different emitting mechanisms, NIR-emitting materials can be divided into fluorescence materials and phosphorescence materials. As shown in Fig. 1(b), fluorescence involves a radiative transition between the same multiple electronic states, i.e., a jump from a ground state to a first excited singlet state or a second excited singlet state. When the electron returns from the first excited singlet state to the ground state, energy is released in the form of light, producing fluorescence.[29] Phosphorescence is produced when the lowest vibrational energy level of the first excited singlet state is transferred to the first excited triplet state by an intersystem crossing, and then, after vibrational relaxation, is transferred to its lowest vibrational energy level and jumps back to the ground state.[30] This process involves a spin-forbidden band transition from the triplet state (T_1) to the ground state (S_0).[29]

In the last decade, organic NIR optoelectronic materials and devices have undergone rapid development. Up to now, a huge number of organic NIR optoelectronic materials have been reported, and the performance of organic NIR optoelectronic devices has improved; many excellent book chapters and review articles on this topic have been published. For example, Cao et al. summarized common molecular design strategies for NIR optoelectronic materials in organic photovoltaics and organic photodiodes.[5] In the field of NIR OSCs, Yang et al. reviewed the donor and acceptor materials used for NIR OSCs in different absorption ranges.[6] Ko et al. discussed the ultranarrow bandgap polymer donors used for NIR OSCs.[31] In the area of NIR OPDs, Ng et al. reviewed polymer-based NIR OPDs.[10] Zheng and Zhu et al. discussed the research progress of organic NIR photodiodes and solution-processable NIR phototransistors, respectively.[16,32] In addition, Liu et al. provided an overview of the development of NIR OPDs from the perspective of organic NIR material selection and device optimization.[33] In terms of NIR OLEDs, topics covered include material design for NIR OLEDs,[34] metal complex-based OLEDs,[35] thermally activated delayed fluorescence (TADF)-based OLEDs,[36] and NIR luminescent materials for use in OLEDs through the collection of triple excitons.[2] For NIR organic lasers, Liao et al. reviewed NIR organic micro/nano lasers and NIR solid-state lasers based on organic small molecules.[12,37] In addition, some reviews on NIR emission materials in OLEDs, organic solid-state lasers (OSSLs), and NIR emission materials based on the excited state

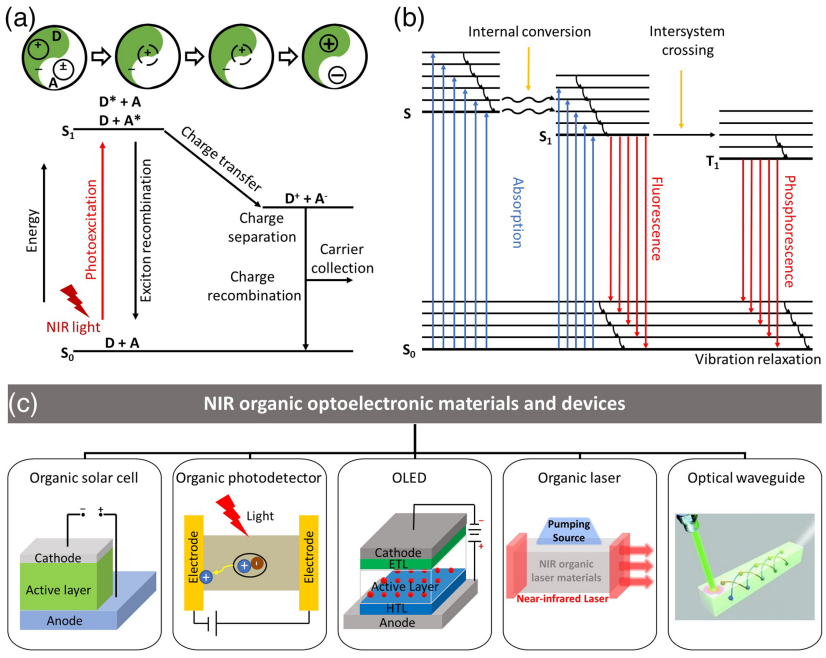

Fig. 1 (a) Mechanism of photogenerated charge transfer. (b) Mechanisms of fluorescence and phosphorescence. (c) Main contents of this review.

intramolecular proton transfer (ESIPT) process have been published.[8,37,38] Although many reviews about organic NIR optoelectronic materials in different devices have been published, none of them emphasized the relationships between subfields, and an overview in this area is still lacking.

In this review, we provide a brief overview of representative organic NIR optoelectronic materials and devices including NIR OSCs, NIR OPDs, NIR OLEDs, NIR organic lasers, and NIR organic optical waveguides [Fig. 1(c)]. In the section on NIR OSCs, we present representative NIR donors and acceptors. After that, we provide an introduction to representative small molecules and polymers in NIR OPDs. Next, for NIR OLEDs, we briefly describe the development of three generations of NIR OLEDs. Then, we give a brief description of dye-doped NIR lasers as well as NIR OSSLs. Moreover, we provide an overview of the development of NIR organic optical waveguides. Finally, after a brief conclusion, we offer an outlook on the development of organic NIR optoelectronic materials and devices.

2 Organic Solar Cells

Due to increasingly serious environment and energy problems, it is urgent that people find alternative green and sustainable energy sources.[39,40] Solar energy is considered one of the most promising energy sources to meet the needs of human society in the future due to its renewable, environmentally friendly, and pollution-free characteristics.[41] Solar cells are devices that convert light energy directly into electrical energy.[42] At present, the commonly used solar cells are silicon-based solar cells,[43] but their manufacturing costs are high, and the manufacturing process is complex.[39] Compared with silicon-based solar cells, OSCs are low cost, lightweight, environmentally friendly, and flexible.[44–47] Formerly, active materials mainly absorbed visible light.[48] However, visible light accounts for 43% of the total energy of the solar spectrum, while NIR light accounts for 52%.[6] Therefore, it is particularly important to develop NIR absorption OSCs. The materials used for OSCs are divided into donor materials and acceptor materials.[49] In this section, we will introduce the representative donor and acceptor materials in NIR OSCs according to the absorption wavelength.

2.1 Donor Materials

In the early stages of OSC development, donor materials were mainly studied,[50–52] but most of the absorption of donor materials was only in the visible light region. With the wide use of fullerene acceptors, donor materials located in the NIR region have been highly developed.[53–57] The properties of representative donor materials and their corresponding device performance are summarized in Table 1. In general, as shown in Fig. 2, donor materials with NIR absorption are D-A type molecules with strong electronic donor units and acceptor units.[68] Among them, thiophene derivatives are commonly used as donor or acceptor units, porphyrins as donor units, and diketopyrrolopyrrole (DPP) and 2,1,3-benzothiazole (BT) as acceptor units to construct materials.[40,69–71] Here, we will introduce representative donor materials based on thiophene, BT, DPP, and thiophene in descending order of absorption window.

2.1.1 NIR donor materials based on thiophene derivatives

Thiophene derivatives are widely used in the NIR absorption region of 760 to 800 nm and are considered the most promising materials to realize narrowband gap materials in the field of OSCs. Among many thiophene derivatives, PBDTTT is the most influential. PBDTTT is composed of benzo [1,2-b: 4,5-b′] dithiophene (BDT) as the donor and thiophene [3,4-b] thiophene (TT) as the acceptor. Wu et al. modified PBDTTT by using different functional groups to adjust its energy level to further adjust the open-circuit voltage by changing the energy level.[58] The highest occupied molecular orbital (HOMO) can be effectively reduced by adding strong electron withdrawing groups to the PBDTTT skeleton. Wu et al. added alkoxy chains and alkyl chains to the carbonyl group of TT to explore the

Table 1 Optoelectronic and photovoltaic properties of representative NIR donor materials in OSCs.

	Donor	E_g^{opt} (eV)[a]	HOMO/LUMO (eV)	Acceptor	V_{OC} (V)[b]	J_{SC} (mA cm^{-2})[c]	FF (%)[d]	PCE (%)[e]	Ref.
Thiophene derivatives	PBDTTT-E	1.61	−5.01/−3.24	$PC_{70}BM$	0.62	13.2	63	5.15	58
	PBDTTT-C	1.61	−5.12/−3.35	$PC_{70}BM$	0.7	14.7	64.1	6.58	58
	PBDTTT-CF	1.61	−5.22/−3.45	$PC_{70}BM$	0.76	15.2	66.9	7.73	58
	PTB7-Th	1.58	−5.22/−3.64	$PC_{71}BM$	0.80	15.73	74.3	9.35	59
DPP-based derivatives	DPPTBI	1.40	−4.87/−3.47	$PC_{61}BM$	0.69	2.02	53	0.74	60
	PDPP3T	1.30	−5.17/−3.61	$PC_{70}BM$	0.66	11.8	60	4.69	61
	PFDPPSe-C18	1.34	−5.46/−3.81	$PC_{71}BM$	0.64	16	60.4	6.16	62
BT-based derivatives	P3	1.34	−5.72/−3.95	$PC_{71}BM$	0.76	6.76	38.6	1.92	63
	PCPDTBT	1.40	−5.30/−3.57	$PC_{71}BM$	0.622	11	47	3.16	64
	PDTP-DFBT	1.38	−5.26/−3.61	$PC_{71}BM$	0.68	17.8	65.0	7.9	65
Porphyrin-based derivatives	CS-DP	1.26	−4.96/−3.74	$PC_{71}BM$	0.781	15.14	69.8	8.29	66
	PPor1	1.18	−5.14/−3.96	$PC_{61}BM$	0.60	11.86	58	4.10	67

[a]Optical bandgap energy.
[b]Open-circuit voltage.
[c]Short-circuit current.
[d]Fill factor.
[e]Photoelectric conversion efficiency.

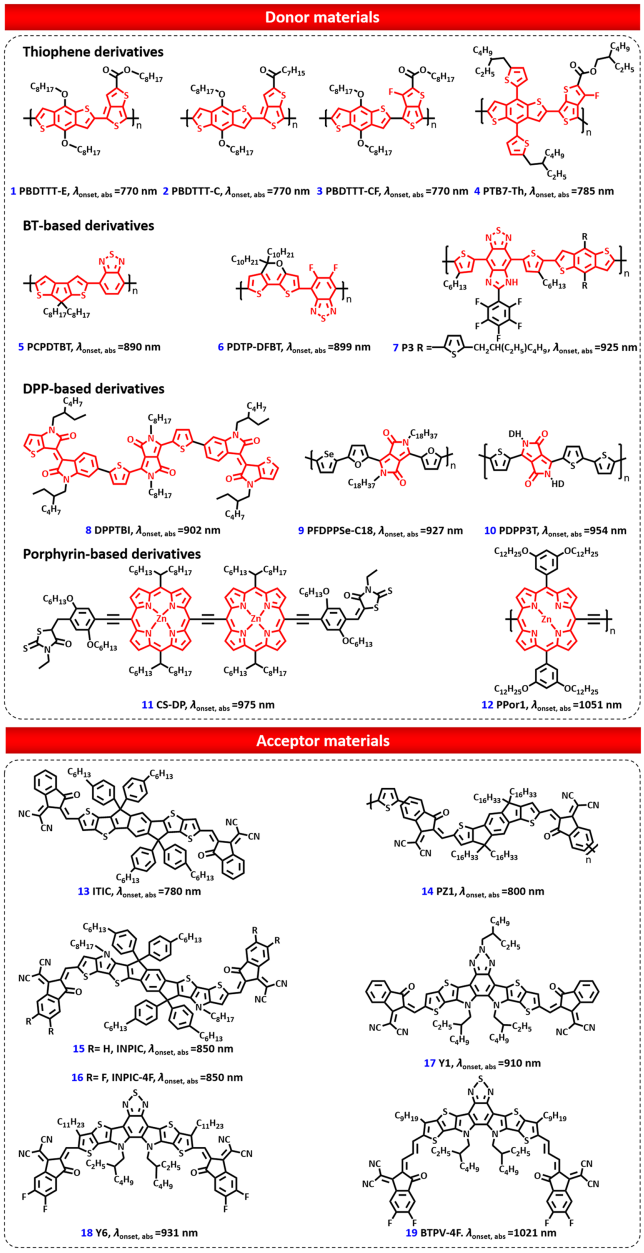

Fig. 2 Typical donor and acceptor materials for NIR OSCs.

effect between them. The results showed that both HOMO and the lowest unoccupied molecular orbital (LUMO) decreased with the modification of the alkyl chain, so the bandgap did not change significantly. In addition, the introduction of fluorine atom into TT made its HOMO and LUMO change, indicating its potential for simple synthetic modification.

In order to achieve redshifted absorption, Chen et al. constructed an influential PBDTTT-type low bandgap donor material PTB7-Th by grafting a 2-ethylhexyl thiophene group onto a BDT unit and a fluorine-substituted TT unit (F-TT) with a 2-ethylhexyl carboxylic acid group.[59] Modification of the 2-ethylhexyl thiophene group enhanced the flatness of the skeleton, resulting in a redshift of the absorption wavelength by ~25 nm. The fluorine-substituted TT unit with a 2-ethylhexyl carboxylic acid group had a higher HOMO.

Due to the outstanding performance of PTB7-Th, Li et al. used it to construct neutral-color semitransparent OSCs.[72] The device structure is shown in Fig. 3(a), in which poly (3,4-ethylenedioxythiophene): poly (styrene sulfonate) (PEDOT:PSS) and mixed Au/Ag were used as electrodes, making the device have less influence on the intensity of transmitted light and spectral components. For the active layer, IHIC with strong NIR absorption capacity was used as the acceptor, and PBDBT/PTB7-Th and J71/PTB7-Th were applied as donor materials to form a terpolymer active layer. Due to the gradient between the bandgap of the donor material and acceptor material, the device exhibited good complementary absorption in the range of 400 to 900 nm. Compared with devices based on the binary active layer J71: IHIC and PTB7-Th:IHIC, the transmission spectrum of devices with the ternary active layer was flatter [Fig. 3(b)], indicating that the added interface layer and top transparent electrode have a uniform transmission spectrum, and the influence on optical components is small when passing through the photoactive layer. In addition, the average visible transmittance (AVT) of three components was equivalent to that of two components, indicating that the third component has little effect on AVT. However, the transmission spectrum of the three components was still very steep, so more long wavelength incident light components were filtered out, making it hard to achieve neutral color devices. In order to make the transmission spectra of the three components more horizontal, 3-DMs composed of three-pair MoO_3/LiF were introduced at the top of the Au/Ag electrode. As shown in Fig. 3(c), the transmission spectrum was obviously leveled after the introduction of 3-DMs. This synergistic effect had good universality, so it can be widely used. More importantly, the ST-OSCs can be applied to power generation windows. As shown in Fig. 3(d), the initial photos of the 3-DMs and the ternary ST-OSCs corresponding to the glass were enlarged. A real window scene was then simulated by cutting out the selected area and reassembling it into a window image for better comparison. It was found that there was no difference between them, proving a potential application in power generation windows.

2.1.2 BT-based NIR donor materials

To make the absorption spectrum over 800 nm, stronger electron donation pairs and electron absorption pairs need to be used. It is a good strategy to achieve absorption beyond 800 nm by introducing various donor units into the BT system.[75–77] For example, Mühlbacher et al. reported the first example of a low-bandgap conjugated polymer PCPDTBT (compound 5) with efficient photovoltaic activity in the infrared spectral region.[64] PCPDTBT used BT as an acceptor and cyclopentadithiophene as a donor, and the polymer showed more favorable charge transport properties, as well as suitable electronic energy levels and good processing properties. When PCPDTBT was mixed with $PC_{71}BM$ to prepare solar cells, the efficiency reached 3.2%. The short-circuit current (ISC) value was 11 mA cm^{-2}, and the EQE reached a maximum of 38% at ~700 nm.

For further redshift of absorption, a low bandgap polymer poly[2,7-(5,5-bis-(3,7-dimethyloctyl)-5H-dithieno[3,2-b:2′,3′-d]pyran)-alt-4,7-(5,6-difluoro-2,1,3-benzothiadiazole)] (PDTP-DFBT, Compound 6) for the construction of tandem solar cells was reported by Yang et al.[65] PDTP-DFBT was prepared based on poly[2,6-(4,4-bis-(2-ethylhexyl)-4H-cyclopenta[2,1-b;3,4-b′]-dithiophene)-alt-4,7-(2,1,3-benzothiadiazole)]. The HOMO was

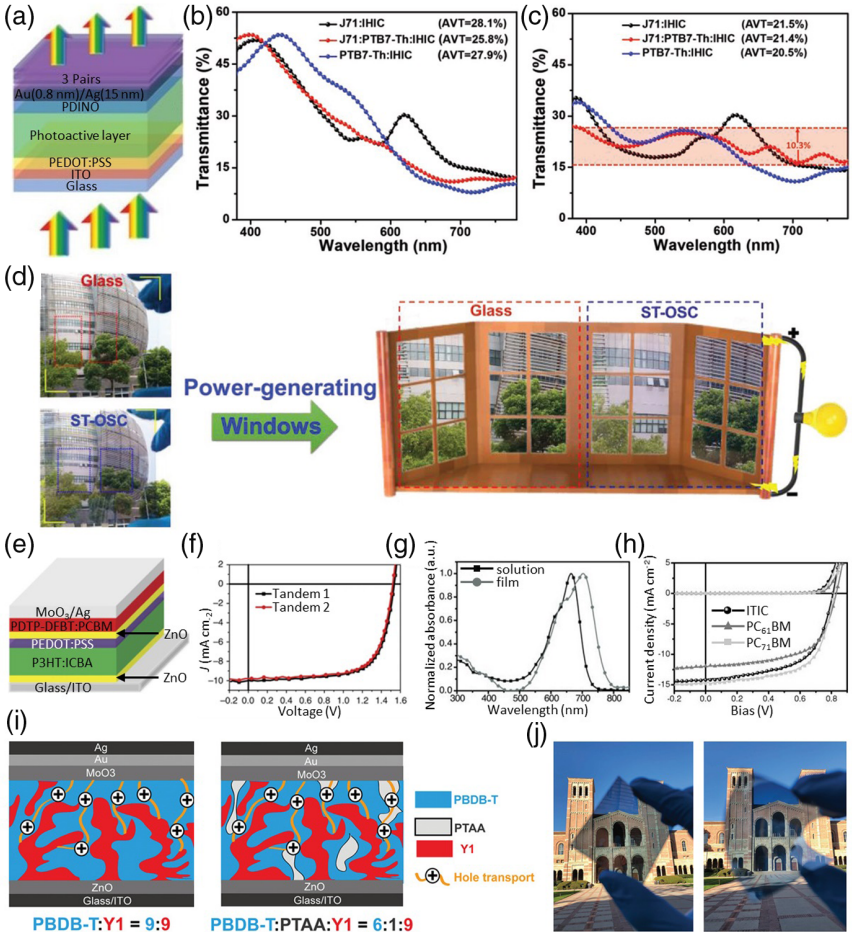

Fig. 3 (a) Device structure combining ST-OSC and 3-DM. (b) Transmission spectra of ST-OSC with different active layers. (c) Transmission spectra of different active layers added with 3-DMs. (d) Photographs of the ternary ST-OSC and glass coating. (e) Schematic diagram of the device structure of the tandem solar cell. (f) $J-V$ curve of Tandem 1 and Tandem 2. (g) Absorption spectra of ITIC in solution (dichloromethane) and films. (h) $J-V$ curves of PSCs with different acceptors. (i) Schematic diagrams of active layers. (j) Optical photograph of a demo [left: glass/ITO/ZnO/PBDB-T:PTAA:Y1 (6:1:9)/MoO3/Au/Ag; right: PET/Ag mesh/PEDOT:PSS PH1000/ZnO/PBDB-T:PTAA:Y1 (6:1:9)/MoO3/Au/Ag]. [(a), (b), (c), (d) Reproduced with permission,[72] © 2019 WILEY-VCH. (e), (f) Reproduced with permission,[65] © 2013 Macmillan Publishers Limited. (g), (h) Reproduced with permission,[73] © 2015 WILEY-VCH. (i), (j) Reproduced with permission,[74] © 2020 WILEY-VCH.]

reduced by introducing two fluorine atoms with electron-absorbing properties into the BT unit to form difluorobenzothiadiazole (DFBT). Next, the energy gap of the polymer was further reduced by the insertion of an oxygen atom into the cyclopentane dithiophene to produce a dithiopyridine (DTP) unit. Subsequently, Yang et al. constructed tandem solar cells using poly-(3-hexylthiophene) with indene-C_{60} bisadduct as the active material for the precell and PDTP-DFBT with $PC_{61}BM$ or $PC_{71}BM$ as the active material for the postcell, where the device containing $PC_{61}BM$ was called Tandem 1 and the device containing $PC_{71}BM$ was called Tandem 2. The device structures are shown in Fig. 3(e). Figure 3(f) shows the $J-V$ curves of Tandem 1 and Tandem 2. From the $J-V$ curves, it can be seen that Tandem 1 has an open circuit voltage (V_{OC}) of 1.53 V, a short circuit current (J_{SC}) of 10.1 mA cm^{-2}, a fill factor (FF) of 68.5%, and a PCE of 10.6%. Tandem 2 has a V_{OC} of 1.51 V, a J_{SC} of 9.80 mA cm^{-2}, an FF of 69.2%, and a PCE of 10.2%. This was the first report of certified polymer solar cell efficiency exceeding 10%, providing a viable strategy for future solar cell efficiency improvements.

Zhang et al. synthesized a fluorine-containing D-A polymer (compound 7) via a Sitlle coupling reaction, resulting in an absorption of over 900 nm.[63] The polymer used a derivative of BT, 5H-imidazo[4,5-f]-2,1,3-benzothiazole (IBT), as an acceptor unit to enhance electron affinity. In addition, electron affinity was further increased by introducing another strong electron absorption unit, pentafluoro phenyl, into the benzimidazole unit, thereby obtaining a larger conjugated skeleton. Moreover, N-H$\cdots$F intramolecular interactions could also hinder the rotation of adjacent thiophene rings, increase the coplanarity and conjugation region of polymers, and reduce the aromaticity of the π system so that the device had better charge transfer and higher PCE. This report provided an effective way to design high-performance D-A polymers based on BT units.

2.1.3 DPP-based NIR donor materials

Since its first report in 1974,[78] due to the strong electron absorption properties, planar geometry, and high hole/electron mobility, DPP derivatives are often used as acceptor units to construct donor materials with absorption above 900 nm by introducing various donor units.[79] Yang et al. constructed the A2-D-A1-D-A2-type small molecular material DPPTBI (compound 8) using DPP as the central acceptor unit (A1), two thiophenes as donors (D), and two benzothiophene isoindoles as the two weaker acceptors (A2).[60] It was found that the addition of thiophene resulted in a redshift of the material spectra; the synthesized materials were highly crystalline. This work provided a new approach to the rational design of small molecule donor materials.

Gunbas et al. reported a polymer PFDPPSe-C18 (compound 9) with NIR absorption up to 927 nm without any thiophene or thiophene-based units in its backbone.[62] The polymer used furan-based DPP as the acceptor and selenylbenzene as the donor. Compared with the analogs containing thiophene, PFDPPSe-C18 showed a broader absorption in the NIR region with a central absorption wavelength of 830 nm and an edge wavelength of 930 nm. Then, PFDPPSe-C18 was used as a donor for OSCs, and after introducing diphenyl ether (DPE) as an additive, high-performance OSCs with PCE over 6% were obtained. More importantly, the NIR absorption capability of PFDPPSe showed promising applications in outdoor windows and translucent devices and was a good candidate for NIR bulk heterojunction (BHJ) bilayer devices.

In another work, Janssen et al. synthesized polymer PDPP3T (compound10) with absorption exceeding 950 nm through the Suzuki reaction.[61] PDPP3T had alternating DPP and thiophene units and an unsubstituted thiophene unit between each pair of DPP units along the chain, which resulted in an enhanced planar type of polymer, thus enhancing stacking and charge carrier mobility. In addition, the DPP unit of PDPP3T had an extended side chain [2-hexyldecyl (HD)], which improved the solubility of the polymer and enabled the polymer with high molecular weight to be obtained. It was found that solar cells prepared by combining PDPP3T with [60]PCBM or [70]PCBM have a photoresponse at up to 900 nm. Moreover, when PDPP3T had a high molecular weight, it had a better efficiency than when it had a low molecular weight, indicating that the molecular weight has a great influence on the efficiency of solar cells.

2.1.4 Porphyrin-based NIR donor materials

Due to the dual absorption peaks, wide absorption range, high absorption coefficient, and easy functionalization of porphyrin-based donor materials, they are often used to construct donor materials with absorption over 950 nm.[40]

Zhu et al. reported a small molecule (CS-DP, compound 11) wrapped in an A-π2-D-π1-D-π2-A type dimeric porphyrin. Two porphyrin monomers in CS-DP were linked via an ethynyl group (π1), and then the porphyrin was connected with the electron deficient group 3-ethylrhodanine (A) by the second acetylbenzene (π2).[66] It was found that the light absorption of CS-DP extends to 975 nm and has a narrow bandgap of 1.22 eV. The solar cell constructed by combining CS-DP and $PC_{71}BM$ with a very small LUMO energy shift between CS-DP had an excellent performance of 8.29% PCE, 15.19 mA cm^{-2} J_{SC}, and 0.796 V V_{OC}. The results showed that dimeric porphyrins with ultrasmall bandgaps had very promising applications in NIR solar cells as well as NIR photodetectors. Li et al. designed and synthesized a small bandgap porphyrin-based conjugated polymer PPor1 (compound 12) with an acetylene-based linker.[67] PPor1 had a strong absorbance in the NIR region because of the cumulative resonance and electronic coupling of the excited states, with absorption up to 1000 nm. In addition, PPor1 showed balanced bipolar charge carrier transport with a hole mobility of 0.0096 $cm^2\,V^{-1}\,s^{-1}$ and an electron mobility of 0.0029 $cm^2\,V^{-1}\,s^{-1}$; the PCE of the OSC based on PPor1 was over 4%. These results showed that porphyrin polymers with quinone structures could be applied to high-quality organic optoelectronic devices.

In summary, this section briefly introduces D-A NIR donor materials based on thiophene, DDP, BT, and porphyrins. In the future, as material properties continue to improve, more high-performance donor and acceptor pairs will continue to be produced, thus allowing NIR energy to be further utilized.

2.2 Acceptor Materials

Currently, the acceptor materials used for NIR solar cells are non-fullerene (NFA) materials. Compared with fullerenes, NFAs have the advantages of coordinated absorption, a high absorption coefficient, structural versatility, low energy loss, and controlled crystallization, which make NFAs widely used in OSCs.[6,80–83] NFA acceptor materials usually have an A-D-A-type structure of a thick-ring electron acceptor (FREA), which is centered on a thick-ring electron donor flanked by two electron-absorbing end groups with an intramolecular charge transfer (ICT) effect.[84] The ICT can be enhanced by tweaking the structure to produce a larger redshift. Based on this, many structural modifications have been adopted to enhance ICT to obtain longer wavelength absorption.[85,86] Optoelectronic and photovoltaic properties of some representative NIR acceptor materials are summarized in Table 2.

In the early stages of development, NIR acceptor materials mainly used indeno[3,2-b]dithiophene (IDT) and indenodithiophene (IDTT) as the donor core. For example, in 2015, a very influential NIR NFA acceptor material, ITIC (compound 13), was reported by Zhan et al.[73] ITIC had IDTT as the donor core and was terminally capped with a 2-(3-oxo-2,3-dihydroinden-1-ylidene)malononitrile (INCN) group and substituted with four 4-hexyl phenyl groups. The electron-absorbing carbonyl and cyano groups in INCN allowed the LUMO of ITIC to be reduced, and the push–pull structure in ITIC induced ICT and prolonged absorption. As shown in the absorption spectrum [Fig. 3(g)], in dichloromethane, ITIC has a strong absorption at 500 to 750 nm. Compared to its solution, the absorption of ITIC in the membrane exhibits a redshift of 38 nm and an intense shoulder peak, indicating the presence of some kind of molecular self-organization in the membrane. This indicates that ITIC has a strong and broad absorption. In addition, by comparing the solar cells constructed with PTB7-Th as the donor and ITIC, $PC_{61}BM$, and $PC_{71}BM$ as the acceptor, it was found that the solar cells with ITIC as acceptor material also show good performance. More importantly, the high PCE of 6.80% is even comparable to typical fullerene-based solar cells, indicating that NFA acceptor materials have great potential for application in solar cells.

To enhance the ICT interaction of the molecule and thus produce longer wavelength absorption, Li et al. reported a new π-conjugated polymer PZ1 (compound 14).[87] PZ1 was composed of n-OS IDIC-C16 as a building block and thiophene as a linker. The effective π-conjugate extension allowed for

Table 2 Optoelectronic and photovoltaic properties of representative NIR acceptor materials in OSCs.

Acceptor	E_g^{opt} (eV)[a]	HOMO/LUMO (eV)	Donor	V_{OC} (V)[b]	J_{SC} (mA cm^{-2})[c]	FF (%)[d]	PCE (%)[e]	Ref.
ITIC	1.59	–5.48/–3.83	PTB7-Th	0.81	14.21	59.1	6.80	73
PZ1	1.55	–5.74/–3.86	PBDB-T	0.83	16.05	68.99	9.19	87
INPIC	1.46	–5.36/–3.82	PBDB-T	0.96	8.55	52.5	4.31	88
INPIC-4F	1.39	–5.42/–3.94	PBDB-T	0.85	21.61	71.5	13.13	88
Y1	1.44	–5.45/–3.95	PBDB-T	0.87	22.44	69.1	13.42	74
Y6	1.33	–5.65/–4.10	PM6	0.83	25.3	74.8	15.7	89
BTPV-4F	1.21	–5.39/–4.08	PTB7-Th	0.65	28.3	65.9	12.1	90

[a]Optical bandgap energy.
[b]Open-circuit voltage.
[c]Short-circuit current.
[d]Fill factor.
[e]Photoelectric conversion efficiency.

better light harvesting and redshift absorption with an absorption coefficient of about 1.3×10^5 cm^{-1}, offering the possibility of constructing a new family of efficient photovoltaic polymer acceptors. Tang et al. inserted sp2-hybridized nitrogen atoms into IDTT to obtain a novel core unit, the fused ring 5,5,12,12-tetra(4-hexylphenyl)-indeno-bis(dithieno[3,2-b:2′,3′-d]pyrrole) (INP).[88] This fused ring had an extended π-conjugated backbone and increased electron donor capacity. Based on INP, Tang et al. constructed two novel NFA acceptors, INPIC (compound 15) and INPIC-4F (compound 16), using 3-(dicyanomethylidene)indan-1-one (IC) and fluorinated IC as end groups, respectively. INIPC and INIPC-4F had a wide and strong absorption in the 600 to 900 nm range owing to the strong electron-donating property of INP. In addition, INIPC-4F showed stronger NIR absorption, with a narrower optical bandgap, better crystallinity, and higher electron mobility than INIPC. In addition, the INPIC-4F-based OSCs exhibited a high PCE of 13.13% and a low energy loss of 0.54 eV. These results indicated that INP had great potential as a donor in the construction of high-performance NFA-acceptor OSCs.

Yang et al. developed a novel NFA acceptor material, Y1 (compound 17), with an A-DA′D-A-type structure, which enabled absorption wavelengths of more than 900 nm.[91] Compared with the A-D-A type acceptor material, Y1 added an electron-absorbing group, 2-ethyl-hexyl-benzo[d]-[1,2,3]-triazole, to the center of the nucleus, thus turning it into a fused D-A′-D structure and enhancing its ICT. In addition, Y1 introduced sp2 hybridized nitrogen atoms with lone pairs of electrons in the core structure to enhance π-domain separation, and finally, Y1 was capped with IC as an acceptor. The use of Y1 for solar cells led to a PCE of up to 12.6%, providing inspiration for the design of next-generation high-performance NFAs and pioneering the study of acceptor materials for Y-series NFAs.

Based on the excellent performance of Y1, Yang et al. also used it in the construction of high-performance semitransparent OSCs.[74] The device structure is shown in Fig. 3(i), where the active layer consists of Y1 as the acceptor and PBDB-T as the donor. In addition, they proposed a unique strategy of a "transparent hole transport framework" by employing a large bandgap polymer for hole transport (poly[bis(4-phenyl)(2,4,6-trimethylphenyl)amine (PTAA)) to partially replace the polymer donor. Since PTAA has a large bandgap, it can reduce the absorption of the active layer in the visible region and maintain the hole transport pathway as well as an optimized film morphology. Based on this strategy, ternary hybrid (PBDB-T/PTAA/Y1) semitransparent devices were realized on both rigid and flexible substrates [Fig. 3(j)].

In 2019, Zou et al. designed a new BT core-based fusion unit of dithieno[3.2-b]-pyrrolo[b]-thiadiazole (TPBT), which could effectively reduce the bandgap and enhance the ICT action, leading to a dramatically redshifted absorption. After that, they designed and synthesized a new Y-series molecule, Y6 (compound 18), which used TPBT and 2FIC units as the central unit and end group and resulted in a further reduction of the energy gap and a further enhancement of the ICT, leading to a further redshift of the absorption spectrum.[89] The molecule showed an absorption edge at 931 nm. Charge transport was facilitated by the formation of noncovalent F-S and F-H bonds to enhance absorption and promote intermolecular interactions. When the polymer PM6 donor was mixed for the preparation of solar cells, the PCE reached a record 15.7%.

In 2021, Li et al. synthesized a new narrow bandgap acceptor BTPV-4F (compound 18) by inserting a double bond between the central core and the terminal group of the Y6 molecule, allowing absorption over 1000 nm.[90] The insertion of the double bond resulted in the extension of the conjugation length and absorption range of BTPV-4F (compound 19). BTPV-4F showed significant redshift absorption covering the range from 600 to 1050 nm. After that, they reported a new n-type π-conjugated polymer PZ1 (compound 19).[87] PZ1 was composed of n-OS IDIC-C16 as a building block and thiophene as a linker. The effective π-conjugate extension allowed for better light harvesting and redshift absorption with an absorption coefficient of about 1.3×10^5 cm^{-1}, offering the possibility of constructing a new family of efficient photovoltaic polymer acceptors. In summary, the NFA acceptor can achieve NIR absorption due to the ICT effect between the donor and acceptor units, and the absorption window of the acceptor can be made to change by selecting different electron-donating ability of the group.

3 Organic Photodetector

Compared with NIR inorganic photodetectors, which are inherently rigid and fragile, complicated to process, and requiring low temperatures, NIR OPDs based on organic small molecules and polymers have advantages such as room temperature operation, easy processing, and compatibility with flexible base

materials.[32,33] Therefore, NIR OPDs have great potential for applications such as electronic products. In order to develop high-performance NIR OPDs, several important aspects need to be considered, such as the NIR absorptivity of the material, the sensitivity, and the response speed of the device.[16,92] Among them, finding suitable materials with efficient absorption in the NIR is an important factor. Currently, a common approach to achieve absorption in the NIR region is to design materials with a low bandgap.[93,94] Over the past few decades, researchers have conducted many studies to extend the spectral response of OPDs to the NIR region and have reported many organic NIR materials for NIR OPDs.[95–97] In this section, we will present representative organic small molecule and polymer materials for NIR OPDs by absorption wavelength. After that, the potential applications of NIR OPDs are briefly described. The structural formula of the presented materials is shown in Fig. 4. The performance of devices based on these materials is shown in Table 3.

3.1 Polymeric Materials for NIR Organic Photodetectors

In 2007, Yang et al. reported the first NIR photodetector based on narrow bandgap polymers.[98] They introduced an ester group at the 2-position of thieno[3,4-b] thiophene to synthesize a novel ester-modified PTT polymer (compound 20) for constructing NIR photodetectors. The introduction of the ester group stabilized the electron-rich thiophene and reduced the HOMO of the PTT to the same energy level as that of PC61BM, thus making it easier to construct devices. In addition, the introduction of ester groups could improve the solubility of the polymer. The absorption peak of PTT was found to be at 750 nm, with an optical bandgap of 1.3 eV. Bazan et al. synthesized PIPCP (compound 21), a narrow bandgap polymer, which had a bandgap of 1.5 eV, by combining two different *D* fragments (indene dithioether and cyclopentanedithiophene) with pyrido[2,1,3]thiadiazole (PT) units.[99] The compound achieved structural control through the precise orientation of the PT fragment relative to the backbone carrier, allowing it to achieve a higher structural order with an absorption peak located at 800 nm. To enable longer absorption wavelengths, a polymer [5,7-bis(4-decyl-2-thienyl)-thiophene(3,4-b) dithiazole-2,5] (PDDTT, compound 22) for high-detectivity photodiodes was reported by Gong et al.[101] The PDDTT not only enabled stabilization of the thiophene chain by introducing the electron-absorbing unit thienopyrazine (TP) but also accelerated the charge and the conjugated backbone. The molecule had a narrow energy system of 0.8 eV, giving it NIR absorption with an absorption peak located at 850 nm.

Later, Müllen et al. reported a D-A type narrow bandgap polymer PPhTQ (compound 23) that absorbs more than 1000 nm.[102] They synthesized PPhTQ by condensing the phenanthrene unit onto the thiadiazinoquinoline fraction. It was found that the optical bandgap of PPhTQ is 0.80 eV; the absorption peak is located at 1143 nm. The compound exhibited good solubility, excellent thermal stability, and well-balanced dipolar charge carrier transport. More importantly, compared with most NIR materials that are too low in carrier mobility to be applied in phototransistors, PPhTQ could be applied in phototransistors because of its good carrier transport. Wudl et al. synthesized another D-A type low bandgap polymer, PBBTPD (compound 24), for organic transistors using benzothiadiazole as the acceptor and dithienopyrrole as the donor.[103] This compound had a low bandgap of 0.6 eV, maximum absorption at 1200 nm, and

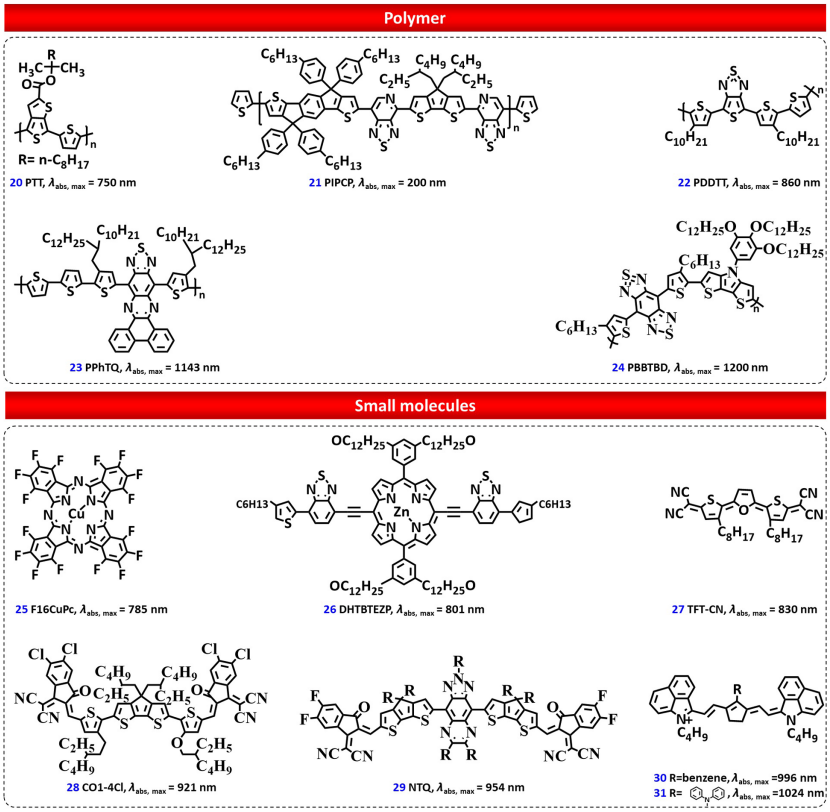

Fig. 4 Representative small molecule and polymer materials for NIR OPDs.

Table 3 Optoelectronic properties for polymer and small molecule absorption materials and devices incorporating them.

	Material	E_g^{opt} (eV)[a]	Spectral region (nm)	$\lambda_{abs,max}$ (nm)	J_d (A/cm^2)[b]	λ_{det} (nm) / V_{bias} (V)[c]	D^* (Jones)[d]	R (A/W)[e]	Ref.
Polymer	PTT	1.30	400 to 970	750	NA	850/–5	NA	0.26	98
	PIPCP	1.50	300 to 1000	800	NA	800/–2	1.34×10^{11}	0.144	99, 100
	PDDTT	0.80	300 to 1450	860	$\sim 10^{-10}$	800/–0.1	2.3×10^{13}	NA	101
	PPhTQ	0.80	700 to 1500	1143	—	—	—	400	102
	PBBTPD	1.44	350 to 2500	~1200	1×10^{-9}	1500/–0.5	2.2×10^{11}	1.4×10^{-7}	103
Small molecule	F_{16}CuPc	1.4–1.5	400 to 800	785	—	—	—	13.6	104
	DHTBTEZP	1.30	380 to 960	801	3.44×10^{-10}	800/0	4.56×10^{12}	NA	105
	TET-CN	1.40	500 to 900	830	—	—	—	9×10^4	106
	CO1-4Cl	1.19	400 to 1100	920	NA	920/–2	10^{12}	0.53	107
	NTQ	1.11	320 to 1070	954	1.5×10^{-5}	980/–2	3.72×10^{12}	0.24	108
	Compound 30	0.80	400 to 1500	1024	1.1×10^{-5}	1390/0	1.7×10^{10}	NA	109
	Compound 31	0.85	400 to 1460	996	1.4×10^{-8}	1140/0	5.3×10^{10}	NA	109

[a]Optical bandgap energy.
[b]Dark current density.
[c]λ_{det} represents the wavelength of the incident light and V_{bias} represents the bias voltage applied on the OPDs.
[d]Specific detectivity.
[e]Responsivity.

good carrier mobility. It was found that mobility may depend on the molecular weight and film mass, but interestingly, not significantly, on the crystallographic order. The formation of tightly packed fine-grained, nonprimary fiber morphologies observed in the polymers suggested that the origin of the high transport properties of the polymers was likely different from many other high-performance polymers that relied on high crystallinity for good transport.

3.2 Small Molecule Materials for NIR Organic Photodetectors

Compared with polymers, organic small molecules have the advantages of easy adjustment of energy levels, high purity, and good reproducibility,[110–112] which gives them good potential for application in NIR OPDs. Among organic small molecules, phthalocyanines have been broadly used in NIR OPDs. In 2007, Zhu et al. prepared phototransistors using submicrometers/nanoribbons of the air-stabilized n-type organic semiconductor F_{16}CuPc (compound 25).[104] The single-crystal field-effect phototransistor with a single submicrometer/nanoribbon of F16CuPc showed a good photoresponse at 785 nm wavelength and exhibited strong light dependence, i.e., incident light could independently control the output current of the transistor. This was the first report of an organic single-crystal-based phototransistor. Peng et al. formed 5,15-bis(7-(4-hexyl-thiophen-2-yl)-2,1,3-benzothiadiazol-4-ylacetylene)-10,20-bis(3,5-di(dodecyloxy)-phenyl)-porphyrin zinc by linking the end of the acceptor 2,1,3-benzothiadiazole (BT) to 3-hexylthiophene (TBT), which was linked by the acetylene group to the porphyrin core (DHTBTEZP, compound 26), which resulted in absorption wavelength up to 800 nm.[105] The molecule exhibited a maximum absorption peak at 801 nm. After that, they prepared solution-treated NIR OPDs using DHTBTEZP as the donor and $PC_{61}BM$ as the acceptor material. The detector could be operated at room temperature with low dark current density and broad spectral response.

For better device performance and longer wavelength absorption, Hu et al. prepared an air-stable ultrathin organic semiconductor two-dimensional (2D) single-crystal film with strong absorption at 830 nm based on TFT-CN (compound 27) and successfully prepared NIR photovoltaic crystals based on this 2D single-crystal film.[106] Compared with most organic NIR photocrystals, NIR photocrystals based on a 2D single crystal film had a lower dark current and a higher detection rate, which provided innovative options for the future development of low-cost, high-performance, and flexible integrated optoelectronics. Furthermore, Nguyen et al. reported a novel NFA acceptor CO1-4Cl (compound 28) with ultrabroadband properties for OPDs.[107] CO1-4Cl had an A-D′-D-D-D″-A conformation, in which cyclopentane dithiophene was used as the central donor (D) unit, with two different thiophene units as subdonors (D′ and D″) and 2-(5,6-dichloro-2,3-dihydro-1H-indenyl) malononitrile as the acceptor (A). The compound had a narrow bandgap of 1.19 eV with maximum absorption at 920 nm. In another work, Chen et al. reported a simple fused-ring nonfullerene acceptor, NTQ (compound 29), with an A-D-A′-D-A framework.[108] NTQ had maximum absorption at 954 nm and a bandgap of 1.11 eV as well as high planarity and high electron mobility. The NTQ-based NIR OPD had a relatively high and balanced hole/electron mobility as well as a high shot noise limit detection rate. This suggested that nonfused acceptors involving multiple D-A effects play an important role in the practical application of NIR photovoltaics. Lunt et al. synthesized two narrow bandgap heptamethyl salts (compounds 30 and 31) for OPDs.[109] The maximum absorption peaks of compounds 30 and 31 were at 996 and 1024 nm, respectively. Counterion exchanged on these heptamethylenimine salts leads to improved performance, which provided a new way to develop low-cost NIR OPDs and efficient multijunction OSCs.

3.3 Potential Applications of NIR Organic Photodetectors

As the performance of NIR OPDs continues to improve, they have great potential for applications in medicine, chemical/biological detection, industry, and many other fields.[18,19,113] NIR OPDs have the potential for use in skin-interfaced health monitoring devices due to their flexibility, nontoxicity, and high penetration in biological tissues.[114] Someya et al. reported an ultraflexible skin conformal photodetector with an NIR response.[100] The device structure of this photodetector is shown in Fig. 5(a). Due to their NIR response characteristics, PIPCP and $PC_{61}BM$ were chosen to form the photoactive layer. Afterwards, an inverted structure was constructed on a polymer substrate (1 μm thick) and passivated using a poly(terephthalic acid) layer (1 μm thick). To minimize failure under mechanical deformation, the device was located in the neutral strain position. They used PIPCP as a donor and $PC_{61}BM$ as an acceptor to form the BHJ active layer. The UV-visible spectrum [Fig. 5(b)] of the device showed two intense absorption fractions at 410 nm (which comes from π-π^* jumps in the polymer backbone) and 800 nm (caused by ICT). The OPDs had been tested and found to have good mechanical durability and operational stability, making them potentially useful as conformal electronic sensors for machine/human interfaces. Based on this, Someya et al. demonstrated a mechanically stretchable, flexible, and skin-conforming photoplethysmogram device by conformal adhesion to a fingerprint curved surface [Fig. 5(c)], which opened up new possibilities for the development of skin-friendly electronics.

In addition to detecting blood pressure, NIR OPDs can also be used in electrocardiographs for real-time heart rate monitoring. Nguyen et al. integrated an NIR OPD into a photocardiograph for real-time heart rate monitoring.[107] Nguyen et al. constructed an OPD using an inverted structure; the device structure is shown in Fig. 5(d). The zinc oxide layer and the BHJ active layer were processed onto a glass substrate with an indium tin oxide layer, followed by a molybdenum oxide layer and a top silver electrode. The BHJ active layer was composed of PTB7-Th as a donor and the ultranarrow bandgap material CO1-4Cl as an acceptor. Due to the presence of CO1-4Cl, the active layer had NIR absorption at 920 nm [Fig. 5(e)]. It was found that the prepared NIR OPDs have high responsivity above 0.5 $A\,W^{-1}$ above 900 nm. In addition, its detectivity D^* at 940 nm was near the noise current of a commercial silicon photodiode, which was 10^{12} Jones. Based on the excellent performance of the photodetector, they performed a simple photoplethysmography test using the OPD, which works as shown in Fig. 5(f). OLED light that was partially absorbed, reflected, and scattered by human tissue could be detected by an optical sensor. Due to the variation in blood volume per cardiac cycle, the method of superimposing various low-frequency signals on the pulsation signal could be used to evaluate the heart rate. This demonstrated the practical potential of NIR OPDs as efficient photodetection platforms.

4 NIR Organic Light-Emitting Diodes

NIR OLEDs have advantages in the development of new "lighting" systems due to their inherent flexibility, large-area application, and compatibility with a wide range of substrates.[34,115] With continuous exploration, OLEDs have undergone three generations of development: the first generation of OLEDs with pure organic fluorescent materials as emitters, the second generation of phosphorescent OLEDs with organometallic complexes as phosphorescent emitters, and the third generation of OLEDs with TADF materials as emitters [Fig. 6(a)].[116] Regardless of the generation of OLEDs, they all aim to improve their external quantum efficiency (EQE), which is a key parameter of OLEDs.[116] In this section, we introduce representative materials and devices in each of the three generations of NIR OLEDs according to the order of electroluminescence wavelengths. The materials to be introduced are shown in Figs. 6(b)–6(d); their respective EQEs are summarized in Fig. 7(a).

4.1 Fluorescent NIR OLEDs

The kinetics of exciton complexation in fluorescent chromophores lasts approximately a few nanoseconds compared to TADF and phosphorescent emitters, making them at least 100 times faster, which makes fluorescent NIR OLEDs an ideal

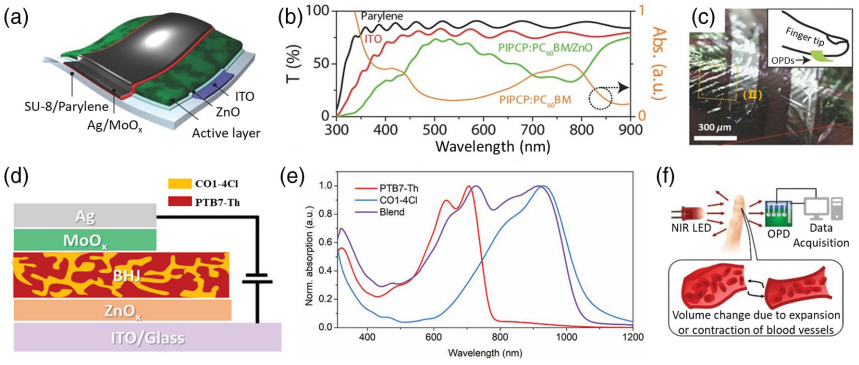

Fig. 5 (a) Schematic of the device structure of ultraflexible NIR OPDs. (b) Transmittance of parylene on different substances. (c) Photograph of fingerprint-conformal NIR OPDs, and the inset indicates the position of the skin-conformal NIR OPDs on the finger. (d) Device structure of the NIR OPDs. (e) Absorption spectra of PTB7-Th (red), CO1-4Cl (blue), and their BHJ blend (purple) in thin films. (f) Working principle of NIR photoplethysmography. [(a)–(c) Reproduced with permission,[100] © 2018 WILEY-VCH. (d)–(f) Reproduced with permission,[107] © 2019 WILEY-VCH.]

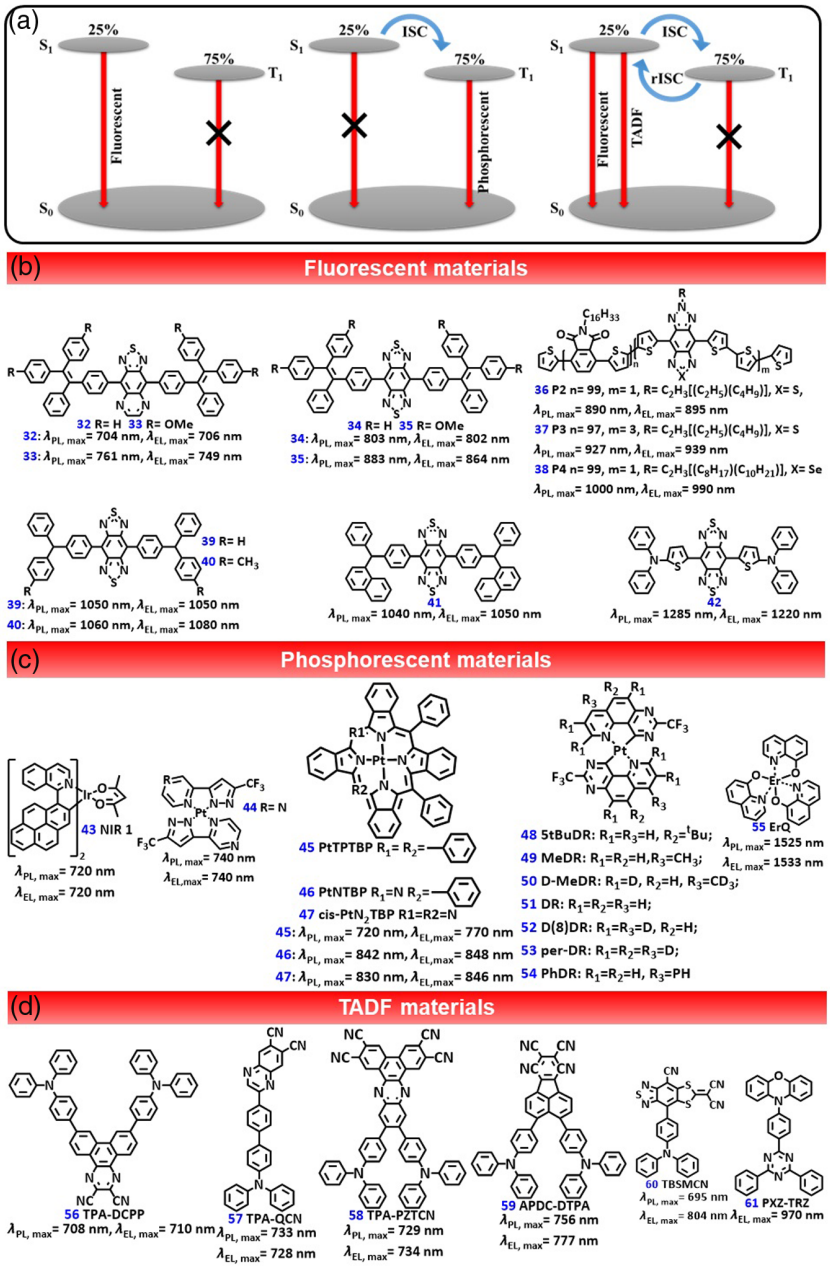

Fig. 6 (a) Mechanism of emitting light of three generations of OLEDs. (b)–(d) Representative NIR materials for each of the three generations of OLEDs.

choice for applications aimed at high transmission rates.[118,119] In addition, compared with phosphorescent OLEDs, OLEDs based on fluorescent materials do not contain metal elements, thus lowering their cost.[120] Here, we give a brief introduction to representative fluorescent NIR OLEDs, whose optoelectronic properties are shown in Table 4.

In 2012, Wang et al. synthesized a series of donor–acceptor–donor (DAD)-type NIR fluorophores (compounds 32–35) containing rigid nonplanar conjugated tetraphenylethylene (TPE) donors.[122] These synthesized molecules all exhibited good aggregation-induced emission (AIE) enhancement properties. Subsequently, nondoped OLEDs based on these compounds were prepared, which showed electroluminescence peaks from 706 to 864 nm, with EQEs ranging from 0.89% to 0.20% and good stability in the current density range of 100 to 300 mA cm^{-2}. Among them, the device based on compound 34 had the best performance, with an EQE of 0.89% and a maximum radiative brightness of 2917 mW Sr^{-1} m^{-2}. In addition, by comparing the undoped and doped OLEDs based on compounds 34 and 36, it was found that the OLEDs with the AIE effect have a higher EQE, thus indicating that AIE compounds were suitable for the fabrication of efficient NIR OLEDs.

To reduce the emission burst and aggregation effects of low-bandgap emitters that induce a redshift in the electroluminescence wavelength, in 2015, Cacialli et al. synthesized P2–P4 by copolymerizing DAD narrow-gap units into a wider-gap host polymer. They copolymerized phthalate-thiophene host

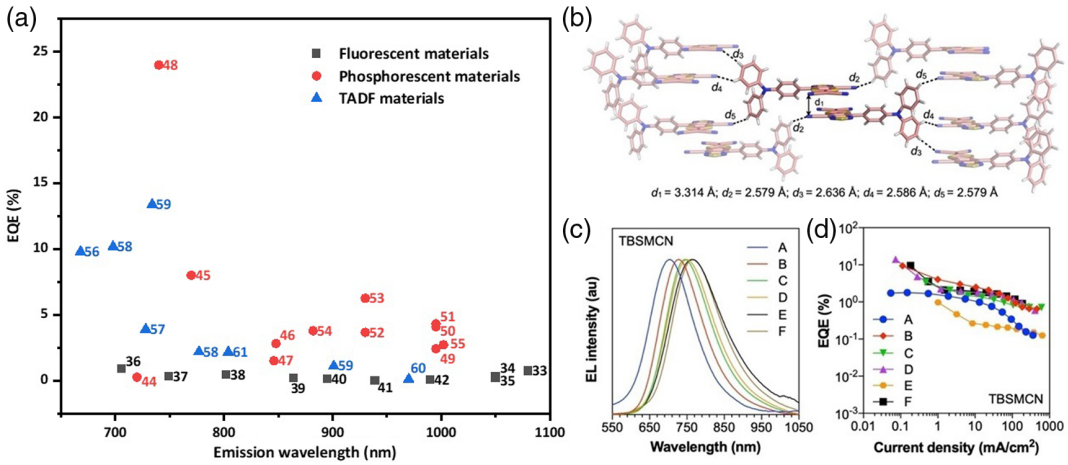

Fig. 7 (a) OLED EQE of the materials mentioned in the article. (b) Crystal structure and intermolecular interaction of TBSMCN. (c) EL spectra of devices with different structures of TBSMCN. (d) EQE of devices with different structures of TBSMCN at different current densities. [(b)–(d) Reproduced with permission,[117] © 2022 WILEY-VCH.]

Table 4 Optoelectronic properties for representative fluorescent materials and corresponding devices.

Compound	$\lambda_{PL,max}$ (nm)[a] (solution/film)	$\lambda_{EL,max}$ (nm)[b]	Φ_{PL} (%)[c]	Max EQE (%)[d]	Ref.
Compound 42	1285/NA	1220	0.5	NA	121
Compound 40	1080/1060	1080	5.8	0.73	121
Compound 41	1040/1040	1050	6.3	0.33	121
Compound 39	1055/1050	1050	7.4	0.16	121
1a	700/704	706	36.9	0.89	122
1b	780/761	749	8.2	0.29	122
2a	787/803	802	0.26	0.43	122
2b	857/883	864	6.39	0.20	122
P240	NA/890	895	NA	0.091	123
P3	NA/927	939	NA	0.006	123
P4	NA/1000	990	NA	0.018	123

[a]Maximum PL peak in solution and thin film.
[b]Maximum electroluminescence peak.
[c]PLQY.
[d]Maximum EQE.

polymers with narrow-gap DAD fractions based on bis-thiophene (benzotriazolyl) units at different loadings to form P2 (compound 36) and P3 (compound 37).[123] In addition, they synthesized P4 (compound 38) by exchanging the sulfur atom in thiadiazole for a selenium atom. It was found that the P2-based OLED had the best efficiency, with an EQE of 0.09%, and showed almost pure NIR luminescence out of the electroluminescence peak at 895 nm, indicating that copolymerization was a successful strategy to obtain purer NIR electroluminescence. P4, which was synthesized by replacing the S atom in the thiadiazole unit of DAD with a Se atom, redshifted the electroluminescence peak to 990 nm, indicating that it was possible to shift the emission further to the NIR by changing the loading of the DAD molecule. Wang et al. synthesized a series of NIR organic chromophores with donor–π–acceptor–π–donor structures (compounds 39–42) that enable electroluminescence beyond 1000 nm.[120] These compounds used benzo(1,2-c:4,5-c0)-bis((1,2,5)-thiadiazole) (BBTD) as the donor, after which BBTD was attached to two electron-donating diarylamino groups via benzene or thiophene units as π-spacers. It was found that the good thermal stability and intense photoluminescence (PL) in the solid state of the prepared compounds make them suitable for application in OLEDs. Based on this, nondoped OLEDs were realized with NIR emission at 1080 nm, an EQE of 0.28%, and the longest electroluminescence wavelength, 1220 nm.

4.2 Phosphorescent NIR OLEDs

Traditional fluorescent emitters can only use 25% singlet excitons for radiation attenuation, while 75% triplet excitons are quenched by thermal radiation.[124] Therefore, NIR OLEDs based

on fluorescent emitters have the disadvantages of low EQE and short operating life. So, harvesting an additional 75% triplet exciton has become an important way to improve light emission. Several methods have been proposed for performing triple exciton harvesting. Among them, using organometallic complexes with phosphorescent emission that can induce the production of spin-orbit coupling interactions as emitters is the most effective method.[35,125,126] The properties of representative materials and devices are shown in Table 5.

In 2006, Jabbour et al. first reported OLEDs with pure NIR emission.[129] The OLEDs were constructed based on Ir complexes Ir (III) bis-(1-pyrenyl-isoquinolinato-N,C′) acetylacetonate (NIR1, compound 43) doped with poly(N-vinylcarbazole) (PVK) and pyrrolobenzodiazepine (PBD) substrates. The electroluminescence peak of this OLED was located at 720 nm; the EQE was close to 0.1%. Moreover, when a hole-blocking layer was used in the structure of the OLEDs, the EQE increased to 0.25%. Chi et al. reported a new 2-pyrazinyl pyrazole salt Pt (II) complex (compound 44) for the construction of NIR OLEDs, resulting in a redshift of the electroluminescence peak of about 20 nm.[131] Compound 44 showed a quantum yield of 81% at the PL peak (740 nm) due to the ordered solid-state stacking arrangement. The structure of the OLEDs was tuned to allow easier exciton formation and recombination in the active layer based on compound 44, which resulted in OLEDs with up to 24% EQE, displaying an electroluminescence peak at 740 nm.

In 2016, Li et al. developed a series of Pt (II) azatetrabenzoporphyrin emitters for NIR OLEDs (compounds 45–47), which resulted in a further redshift of the electroluminescence wavelength.[130] Among them, the electroluminescence peak of PtTPTBP (compound 45)-based OLEDs was located at 770 nm with an EQE of 8.0%, while PtNTBP (compound 46)- and cis-PtN2TBP (compound 47)-based OLEDs showed redshifted electroluminescence emission; their emission peaks were located at 848 nm (EQE of 2.8%) and 846 nm (EQE of 1.5%). This suggested that replacing the medium carbon group with a nitrogen group in the porphyrin ring could be an effective strategy for color tuning.

Recently, Chou et al. reported a novel class of self-assembled Pt (II) complexes that overcame the energy gap law to achieve NIR luminescence at ∼1000 nm and increased the quantum rate of emission to >20% by deuteration of C-H.[132] Based on 8-(trifluoromethyl)pyrido[2,3-f]quinazoline (pnazH), they designed and synthesized a new chelate, coupled them with K_2PtCl_4 to obtain Pt (II) emitters DR (compound 51), MeDR (compound 49), 5tBuDR (compound 48), and PhDR (compound 54), and deuterated them to obtain D(8)-DR (compound 52), per-DR (compound 53), and D-MeDR (compound 50). Due to the synergistic effect of the self-assembled exciton leaving domains, all compounds had NIR electroluminescence emission over 800 nm. After that, they prepared OLEDs based on each compound, where the EQEs of the MeDR-, 5tBuDR-, and PhDR-based OLED devices were 3.66%, 3.78%, 2.42%, and 2.71%, respectively. Because the internal conversion rate of deuterium reduces and eliminates the high-frequency vibration related to C-H and suppresses the overlap of F-C, OLEDs based on D(8)-DR, per-DR, and D-MeDR showed higher EQE (4.08%, 4.31%, and 6.25%, respectively). In addition, deuterium substitution also led to a corresponding increase in the PL quantum yield (PLQY) from 13.3% (compound 51) to 19.5% (compound 52) and 22.8% (compound 53). This work provided a new idea for the preparation of high-quality NIR emitters and OLEDs. In addition, Curry and Gillin used erbium-doped erbium (III) tris,8-hydroxyquinoline (ErQ, compound 43) as the emitting layer of the OLEDs, showing an electroluminescence peak at 1.54 μm.[127,128] The results suggested a possible route to produce a silicon-compatible 1.54 μm source technology. With more in-depth studies, it was found that OLEDs constructed by mixing metal complexes in a host matrix could achieve more efficient NIR electroluminescence.

Table 5 Optoelectronic properties for representative phosphorescent materials and corresponding devices.

Compound	$\lambda_{PL,max}$ (nm)[a]	$\lambda_{EL,max}$ (nm)[b]	Φ_{PL} (%)[c]	Max EQE (%)[d]	Ref.
ErQ	1522	1533	NA	NA	127, 128
NIR 1	720	720	NA	0.25	129
PtTPTBP	770	770	51.0	8.0	130
PtNTBP	842	848	22.0	2.8	130
cis-PtN_2TBP	830	846	17.0	1.5	130
Compound 48	740	740	81	24	131
DR	965	995	13.3	2.42	132
D(8)-DR	965	995	19.5	4.08	132
per-DR	965	995	22.8	4.31	132
MeDR	920	930	16.0	3.66	132
D-MeDR	920	930	26.0	6.25	132
5tBuDR	855	882	18.1	3.78	132
PhDR	970	1002	13.2	2.71	132

[a]Maximum PL peak.
[b]Maximum electroluminescence peak.
[c]PLQY.
[d]Maximum EQE.

4.3 Thermal Activation Delayed Fluorescence NIR OLEDs

Although phosphorescent OLEDs can theoretically achieve 100% exciton utilization, the presence of heavy metals makes the cost of phosphorescent OLEDs high and thus unfavorable to commercialization.[133] In addition, heavy metals also cause environmental pollution, which is not conducive to sustainable and healthy development. Therefore, the search for new OLEDs that can be used as an alternative to phosphorescent OLEDs has attracted extensive research interest. Recently, TADF-based OLEDs have been considered the most promising alternative. The small energy difference between the lowest energy excited singlet state (S1) and the lowest energy excited triplet state (T1) of the TADF allows 75% of the triplet excitons to be converted from T1 to S1 via a thermally activated reverse intersystem crossover (RISC) process, thus allowing 100% exciton utilization of the TADF material.[134,135]

Many red, green, and blue OLEDs based on TADF materials with high EQE have been reported,[136–138] but fewer OLEDs based on NIR TADF materials with high EQE have been reported (Table 6). This is because, according to the energy

Table 6 Optoelectronic properties for TADF materials and corresponding devices.

Compound	ΔE_{ST} (eV)[a]	$\lambda_{PL,max}$ (nm)[b]	$\lambda_{EL,max}$ (nm)[c]	Φ_{PL} (%)[d]	Max EQE (%)[e]	Ref.
TPA-DCPP	0.13	708	668	14	9.8	139
TPA-QCN	0.23	733	728	21	3.9	140
APDC-DTPA	0.14	687, 756	698, 777	63 (@687 nm), 13 (@756 nm)	10.19 (@693 nm), 2.19 (@777 nm)	141
PXZ-TRZ	NA	NA	970	0.3	0.1	142
TPA-PZTCN	0.14	729	734, 901	40.8	13.4 (@734 nm), 1.1 (@901 nm)	143
TBSMCN	0.17	820	804	10.7	2.17	117

[a]Difference between singlet and triplet energies.
[b]Maximum PL peak.
[c]Maximum electroluminescence peak.
[d]PLQY.
[e]Maximum EQE.

gap law, when the energy gap of a luminescent material becomes narrower and enters the deep-red or NIR region, the vibrational relaxation of the singlet and triplet states is accelerated, resulting in a sharp increase in the nonradiative rate, which greatly reduces the radiative rate and thus has a great impact on its fluorescence efficiency.[34,36]

With the continuous exploration of researchers, certain developments have been made in TADF-based NIR OLEDs. The first NIR OLED based on TADF material was reported by Wang et al. in 2015. They synthesized a D-π-A-π-D conformation of the V-shaped molecule TPA-DCPP (compound 56).[139] TPA-DCPP had a small ΔE_{ST} of 0.13 eV and a large fluorescence rate of 9.0×10^{-7} s^{-1}. The nondoped OLED based on this molecule showed an electroluminescence peak at 710 nm with a maximum EQE of 2.1%, which provided a new approach to design efficient organic NIR fluorescent molecules. To further redshift the electroluminescence spectrum, in 2017, Wang et al. synthesized the TADF compound TPA-QCN (compound 57) with a D-π-A type.[140] Compound 57 used TPA as the electron donor and quinoxaline-6,7-dicarbonitrile (QCN) as the acceptor, and its skewed π-conjugated structure and potential intermolecular forces pointing to the edges of the QCN molecule allowed TPA-QCN to aggregate in an edge-to-edge manner, thus avoiding π-π stacking and allowing the luminescence to be redshifted, resulting in a 733 nm NIR emission in the film. Subsequently, NIR-emitting OLEDs were obtained by pure film preparation of TPA-QCN with the electroluminescence peak located at 728 nm. The EQE was 3.9%, indicating that high-performance NIR OLEDs could be obtained by reasonable molecular design.

Later, Adachi et al. reported a TADF material (TPA-PZTCN, compound 58) with V-shaped structure and multiband NIR emission.[143] The molecule was composed of dibenzo[a,c]phenolizine-2,3,6,7-tetracarbonitrile (PZTCN), with high molecular rigidity as an acceptor and two TPAs as donors. The NIR OLEDs based on this molecule showed two electroluminescence peaks located at 734 and 901 nm. In addition, the NIR OLEDs had high EQE values of 13.4% and 1.1% at 734 and 901 nm, respectively, which provided a promising strategy for the development of efficient dual-band NIR OLEDs. Liao et al. reported a TADF material, APDC-DTPA (compound 59), which was structurally similar to TPA-DCPP but with a redshifted electroluminescence peak of about 70 nm.[141] Compared with TPA-DCPP, APDC-DTPA used acenaphthene- [1,2-b]-pyrazine-8,9-dicarbonitrile (APDC) as an acceptor, resulting in a redshifted spectrum. The nondoped OLEDs based on APDC-DTPA showed excellent performance, with a maximum EQE of 2.19% and an electroluminescence peak at 777 nm.

To achieve an electroluminescence peak of 800 nm for OLEDs, an electron-deficient acceptor BSM based on dithiolated fullerenes and benzothiadiazoles was designed and synthesized by Tang et al.[117] This acceptor could be used to construct NIR-emitting materials with AIE properties. Based on BSM, they synthesized TBSMCN (compound 60), a TADF material with AIE properties, using TPA as a donor, which had a PL peak of 820 nm in the film. After that, they obtained their TBSMCN single crystals by the slow evaporation method, whose molecular arrangement is shown in Fig. 7(b). The TBSMCN single crystals had π-π and D-A interactions, resulting in a redshift in their spectra compared to their thin films (PL > 850 nm). After that, they prepared doped and nondoped OLEDs based on TBSMCN by a solution treatment method. The nondoped OLEDs showed 2.2% EQE at 804 nm, which was excellent for nonrare metal NIR OLEDs in this spectral range. For their doped OLEDs, they maximized the EL performance by introducing a doping configuration with a host (mCP) and sensitizer. Figures 7(c) and 7(d) show the EL spectra and EQE of the different doped OLEDs. Devices A-C were prepared based on different concentrations of TBSMCN solution in mCP (A: 5%, B: 25%, C: 50%). The EL peaks gradually redshifted with increasing concentration, and the highest EQE of 9.4% was shown in device B with a 25% doping concentration (EL peak at 728 nm). Devices D and E, on the other hand, obtained triple excitons by introducing the TADF polymer PCAQC0.5, iridium complex Ir-$(MDQ)_2$(acac), and red quantum dot Nato-R, respectively. Among them, device D showed the best performance, with an EQE of 14.3% at 750 nm.

In 2017, an OLED with electroluminescence exceeding 950 nm was reported by Adachi et al.,[142] which could efficiently collect triplet state energy through RISC in the TADF body layer, thus using the electrically generated exciton energy almost exclusively for NIR phosphorescence. They obtained mixed electroluminescence peaks up to 1100 nm using the TADF material PXZ-TRZ (compound 61) as the host substrate for RISC and copper phthalocyanine (CuPc) and platinum phthalocyanine (PtPc) as NIR phosphorescent materials.

Although metal phthalocyanines had a relatively low phosphorescence efficiency, which made the EQE of metal phthalocyanine-based OLEDs below 0.1%, this obstacle could be overcome by using highly emissive NIR phosphorescent materials.

5 NIR Organic Laser

Since the first report of lasers in 1960,[144] lasers have attracted extensive research interest due to their unique luminescent properties, such as coherence, directionality, monochromaticity, and high intensity.[21] Among them, NIR lasers have received much attention for their potential applications in sensing, display, and photonic integrated circuits.[145–147] Typically, a laser consists of a gain medium, a pumping source, and an optical feedback structure.[148] Among them, the gain medium is the key component in the laser. Since the first report about them in 1966,[149] lasers with organic dyes as gain media have attracted extensive attention due to the tunable chemical structures of organic dyes, simple preparation processes, and large stimulation emission cross section.[150–152] With continuous development, organic dye lasers have showed the advantages of tunable wavelength range, high output power, easy control of absorption and gain, and continuous wave generation.[37,153,154] Compared with traditional liquid organic dye lasers, organic solid-state dye lasers are widely used because of their high efficiency, small size, and reduced health and environmental hazards. But they have problems, such as high defect density, low optical gain, and poor stability. In contrast, organic single crystal lasers have received widespread interest recently due to their low defects, high optical gain, and good stability.[155–157]

In this section, we give a brief introduction to different types of NIR OSSLs based on the laser wavelength, including organic dye-doped and organic crystal-based NIR organic lasers. The properties of the two types of organic NIR lasers are shown in Table 7.

5.1 Organic Dye-Doped NIR Organic Lasers

Although NIR organic lasers have come a long way, they still have disadvantages, such as low stimulated emission and exciton–exciton annihilation due to high pump intensity.[37,153] Usually, NIR gain materials are often doped in the host substrate to obtain a high optical gain and low laser threshold to overcome these disadvantages. Among various host substrates, the use of metal–organic frameworks (MOFs) as host substrates can inhibit concentration quenching and exciton–exciton annihilation by encapsulation and space separation of dye molecules. Hu et al. realized the NIR microscale laser at room temperature by doping organic dye LDS 798 [compound 62, molecular structure as shown in Fig. 8(a)] into the MOF cavity.[162] As shown in Fig. 8(b), they successfully introduced LDS 798 into rho ZMOF microcavity through the ion exchange method. The space limitation of LDS798 in the pores helped to minimize the intermolecular interaction and exciton annihilation. This enabled a single LDS 798@rho-ZMOF. The multimode NIR laser with microcrystal ≈790 nm had a quality factor (Q) as high as 1863 [Fig. 8(c)], which showed a new way to realize an organic NIR solid laser in a single MOF crystal.

In addition to MOFs as substrates, organic small molecules are often used as host substrates because of their ability to reduce aggregate quenching of laser dyes.[37] A typical example is the low-threshold NIR (ASE) activity of coblended membranes prepared by doping with different concentrations of TADF curcumin derivatives (compound 63), using 4,4′-bis(N-carbazolyl)-1,10-biphenyl (CBP) as the main substrate, as demonstrated by Adachi et al.[160] The structure of compound 63 is shown in Fig. 8(d1). When the doping concentration reaches 4% (mass fraction), the coblended film exhibited the NIR ASE phenomenon with a peak at 740 nm. In addition, the ASE peak gradually redshifted (from 740 to 799 nm) as the doping concentration

Table 7 Properties of NIR OSSLs.

	Material	$\lambda_{PL,max}$ (nm)	$\lambda_{laser,center}$ (nm)	Threshold ($\mu J\,cm^{-2}$)	Ref.
Dye-doped NIR laser	LSD950/FPI	960	970	220	158
	ADH/PS	750	860	27.4	159
	Compound 63/CBP	706 to 782	740 to 799	~5 to 37	160
	Compound 64/CBD	751 to 801	801 to 860	7.5 to 91.4	161
	LDS 798/rho ZMOF	~750	790	17.2	162
NIR laser in crystal state	DMHAC	710	714	9.2 $kW\,cm^{-2}$	163
	Compound 68	716	716	100 $kW\,cm^{-2}$	163
	DFHP	702	714	20.8 $kW\,cm^{-2}$	164
	DPHP	596	700	0.61 (TM mode), 0.75 (TE mode)	165
	DMHP	675	720	1.4	166
	DEPHP	700 (α-phase), 728 (β-phase)	730	1.86	167
	DMHC	700	775	9.9	168
	DDMP	778	854	13.2	169
	TPE-SP	660	720	3.68	170
	DP-DHAQ	660	725	26.9	171
	H_2TPyP	655 (0-0), 716 (0-1)	732	0.119	172

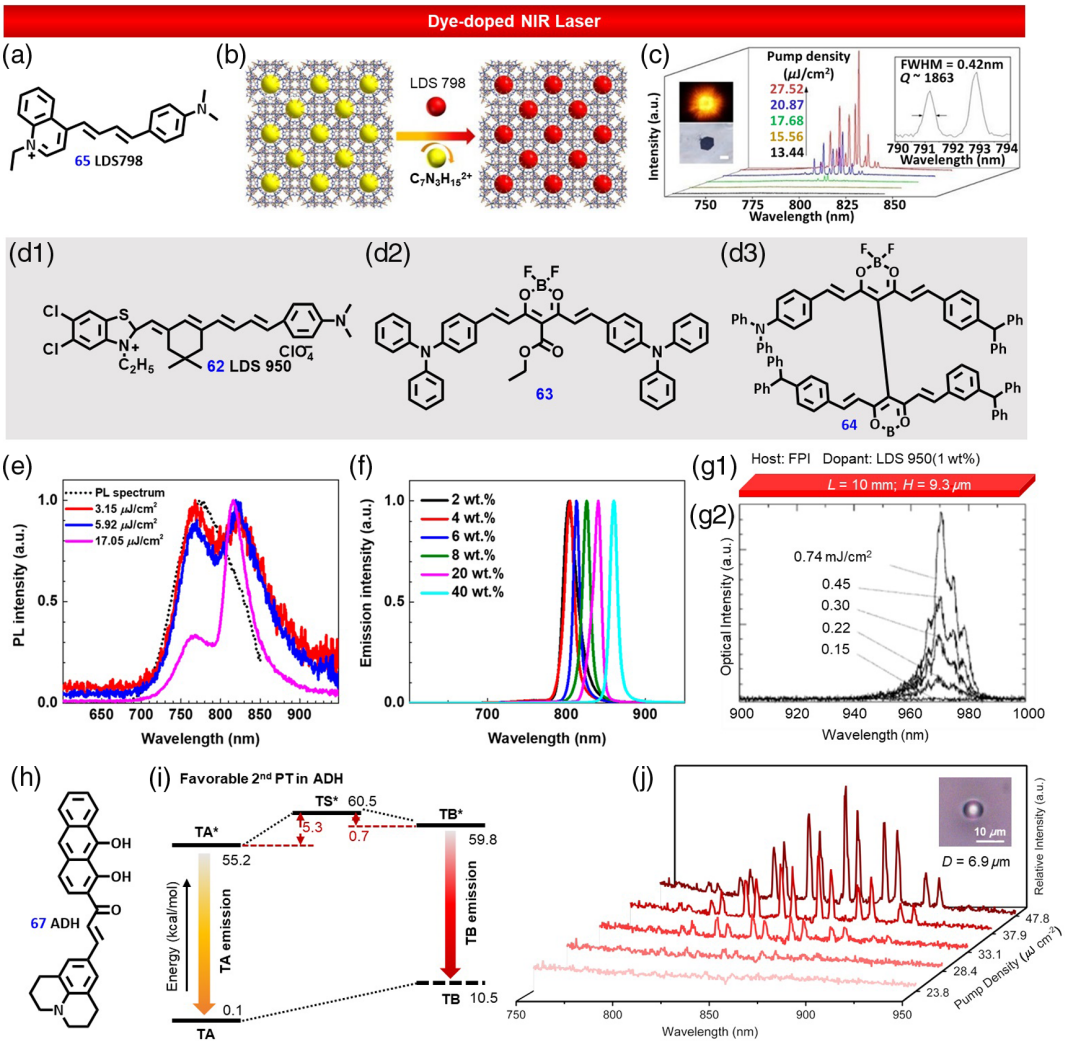

Fig. 8 (a) Molecular structures of LDS 798. (b) Schematic illustration of the formation of LDS 798@rho-ZMOF microcrystals via an ion exchange process. (c) Room-temperature PL spectra of an individual LDS 798@rho-ZMOF microcrystal under different pump densities at 532 nm. (d1)–(d3) The molecular structures of compounds 64, 65, and 66. (e) PL spectra of compound 64 in doped films at different pumping energies. (f) Laser emission spectra of compound 64 in doped films of different concentrations. (g1) Schematic diagram of the dye-doped film. (g2) The lasing emission spectra from the active waveguide with the FP cavity at increasing excitation levels near the threshold. (h) Molecular structure of ADH. (i) Calculated relative energies (kcal mol^{-1}) of the TA and TB forms of NDH. (j) Laser emission spectra of ADH in PS spheres. [(b), (c) Reproduced with permission,[162] © 2018 American Chemical Society (ACS). (e), (f) Reproduced with permission,[161] © 2018 ACS. (g2) Reproduced with permission,[158] © 2008 American Institute of Physics. (i), (j) Reproduced with permission,[159] © 2020 WILEY-VCH.]

increased (from 4% to 60%, mass fraction), indicating that a tunable NIR ASE can be achieved. In another work, the same group achieved tunable NIR ASE at longer wavelengths from 801 to 860 nm by doping another boron difluoride curcumin derivative [compound 64, molecular structure shown in Fig. 8(d2)] in CBD.[161] As shown in Fig. 8(h), with the increase in pump energy, its spectrum gradually narrows, indicating that it has the ASE phenomenon. More importantly, when the doping concentration gradually increased from 2% to 40% (mass fraction), the peak value of NIR ASE gradually redshifted from 801 to 860 nm, indicating the potential application of boron difluoride curcumin derivatives in NIR organic semiconductor lasers [Fig. 8(i)].

In addition to the above two kinds of host substrates, polymers have been widely used as substrates due to the better solubility and greater optical gain of organic dyes in polymeric substrates.[173] For example, Liao et al. achieved a six-level system laser toward 900 nm by doping molecules with ESIPT activity into polystyrene (PS).[159] They designed and synthesized the ESIPT active molecule ADH using anthracene as the

molecular backbone [Fig. 8(h), compound 66]. By calculating the relative energy of S_0 and S_1 of ADH, it was found that the first ESIPT process (N* → TA*) was barrier-free. Although there was a transition state for the second proton transfer (PT) process, the energy of the TB* was lower than that of the transition state, so it could still carry out the second transfer [Fig. 8(i)]. In S_0, the first reverse PT process (TB → TA) was also calculated as barrier-free. In the second reverse PT process (TA → N), the difference in energy between TA and N was not significant. Therefore, ADH could form a six-level system to provide longer wavelength emission. After that, they doped ADH in PS to make PS microspheres test their laser performance. Figure 8(j) shows the morphology of the prepared microsphere and the laser spectrum of a single PS microsphere at different pump energies. Its central wavelength was located at 860 nm, and it also has a laser peak at 900 nm, which was the longest luminescence wavelength based on ESIPT active gain material. This work provided an effective molecular design strategy for the realization of a six-stage system laser.

Oe et al. doped the organic dye LDS950 (compound 65) in fluorinated polyimide (FPI), thereby achieving NIR lasers at ~970 nm on FPI planar waveguides.[158] Figures 8(d3) and 8(g1) show the molecular structure of LDS 950 and the schematic diagram of the FPI planar waveguide, respectively, where the FPI planar waveguide had a length of 10 mm and a thickness of 9.3 μm, doped with 1% (mass fraction) of LDS 950 dye. Figure 8(g2) shows the emission spectra of the active waveguide with the FP cavity at different pump energies. It can be seen that it showed a strong laser peak at 970 nm with increasing pump energy. This result was the longest wavelength for the dye-doped polymer laser and demonstrates the superiority of the dye-doped NIR laser based on the polymer matrix.

5.2 NIR Laser in Crystal State

Compared with organic dye-doped NIR organic lasers, organic crystals are favorable candidates for gain materials because of their regular shape, fewer defects, and high gain density.[148,156,174] Zhang et al. reported a series of NIR light-emitting organic crystals based on 2′-hydroxychalcone [compounds 67, 68, Fig. 9(a)] through a simple condensation reaction, and these crystals showed extremely low threshold ASE.[163] As shown in Figs. 9(b1) and 9(b2), compounds 67 and 68 showed ASE characteristics at different pump energies, with peak values of 714 nm (compound 67) and 716 nm (compound 68), respectively. Later, the same group reported an NIR material DFHP (compound 69) with a similar structure.[164] Based on DFHP, they prepared two polymorphs 1O (α-phase) and 1R (β-phase) with ASE. Furthermore, when heating 1R to 130°C, it could be converted from β-phase to α-phase [Fig. 9(c)]. The emission peaks of 1R and 1O were located at 702 and 618 nm, respectively. In addition, the emission of 1R at 714 nm gradually narrowed and amplified with increasing pump energy, indicating the realization of ASE [Fig. 9(d)].

Many NIR laser materials based on 2-acetyl-1-naphthol derivatives have been reported. For example, Fu et al. self-assembled microspheres through DPHP [compound 70, Fig. 9(e)].[165] The microspheres exhibited NIR lasing at ~700 nm and had an ultralow threshold of 610 nJ cm^{-2}. In addition, the laser stability of the microspheres was also excellent, and the laser intensity had almost no change within 20 min. Later, the same group reported two NIR materials with similar structures, DMHP (compound 71) and DEPHP (compound 74), resulting in laser wavelengths redshifted by 20 and 30 nm, respectively.[166,167] For DMHP, nanowires were prepared by the solution exchange method. By adjusting the length of the nanowires, tunable lasers at 660 and 720 nm were realized. For DEPHP, the α phase with dark red emission and the β phase with NIR emission were prepared by the solution exchange method. Moreover, the β phase exhibited an ASE phenomenon at 730 nm with a threshold as low as 1.86 μJ cm^{-2}. More importantly, resonant laser peaks were also observed in single crystals in the β phase, indicating that it can be used as resonant cavities in lasers.

In 2020, Liao et al. reported a nanolaser array with a 775 nm NIR laser at room temperature. The nanoarrays consisted of organic nanowires obtained from small-molecule DMHC (compound 76) preparation; the prepared single-crystal nanowires and nanolaser arrays are shown in Figs. 9(g) and 9(h), respectively.[168] The laser spectra of nanowires at different pump energies are shown in Fig. 9(i). It shows an NIR laser at 775 nm with a threshold of ~9.9 μJ cm^{-2} and a quality factor Q of ~2340, indicating that the nanowire had good optical feedback. Importantly, this was the first report on nanolaser arrays above 760 nm at room temperature. To realize lasing above 800 nm, DDMP (compound 77), an NIR material with excited-state double PT property, was designed, which can be used to construct a Fabry–Perot cavity.[169] Under excitation, the first PT could proceed within 430 fs, followed by a second major and irreversible PT in 1.6 ps. After that, they prepared nanowires of the material by the solution exchange method. The prepared nanowires can act as a laser medium and a resonant cavity at the same time. It showed an NIR laser signal near 854 nm [Fig. 9(f)]. This work led to the optimization of the cascaded six-level system and provided a new idea for the establishment of the energy level system of NIR organic lasers.

In addition to 2-acetyl-1-naphthol derivatives, other types of NIR micro/nanocrystal lasers have been reported. The first low-threshold NIR microlaser based on self-assembled microsphere caps of spiropyrane (SP) was reported by Zhao et al.[170] They prepared TPE-SP (compound 72) by combining highly distorted TPE with SP molecules. The addition of TPE made the free volume large enough to facilitate the photoisomerization process and weakened the intermolecular π-π stacking to enhance the solid-state NIR emission. The self-assembled microsphere cap based on TPE-SP could be used as both a gain medium and a resonant microcavity, thus achieving an ultralow threshold NIR microlaser with 3.68 μJ/cm^2 at 720 nm, which provided a way to build a new type of microlaser. Recently, Liao et al. reported DP-DHAQ (compound 73), a material for NIR ESIPT with resonance-assisted hydrogen bonds (RAHBs).[171] The presence of RAHBs could activate the ESIPT laser by suppressing nonradiative decay, thus enabling a single crystal sheet based on DP-DHAQ to achieve an NIR laser with 725 nm emission [Fig. 9(j)], which provided a new proposal for the design of organic laser-active molecules. In addition, Yoon et al. observed NIR lasers for the first time in single-crystal rectangular microtubes prepared on the basis of tetra(4-pyridyl)-porphyrin (H_2TpyP, compound 75).[172] Rectangular microtubes were prepared by the evaporation–condensation–recrystallization method with two optical resonant cavities, a Fabry-Perot mode in the extended degree direction, and a rectangular ring mode along the corners of the ports, resulting in an NIR laser at 730 nm.

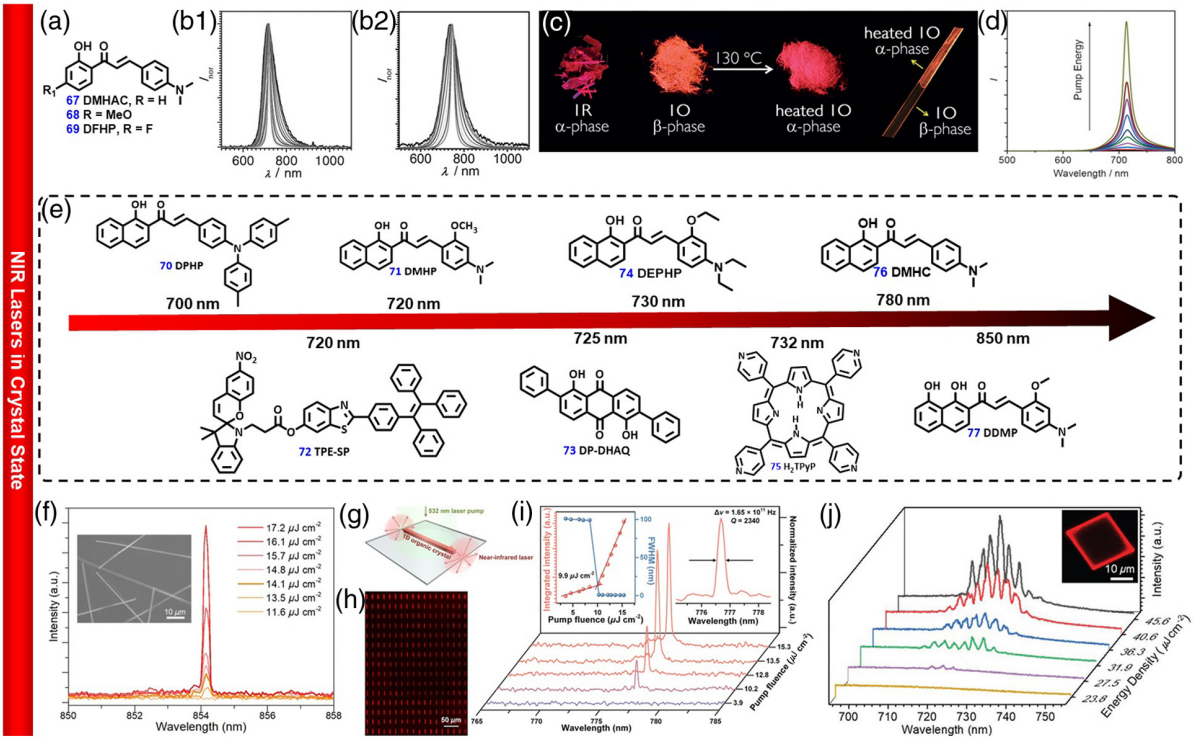

Fig. 9 (a) Molecular structures of 67, 68, 69. (b1), (b2) PL spectra of compounds 67 and 68. (c) Images of 1R, 1O, heated 1O, and the heated phase transition of 1O. (d) PL spectra of 1R. (e) Chemical structures of representative materials. (f) PL spectra of 11.5 μm long single nanowires excited by different pump energies. Inset: SEM image of organic nanowires. (g) Schematic of one nanowire on a glass substrate pumped by 532 nm laser excitation. (h) Fluorescence microscopy image of these as-prepared DMHC organic nanowire arrays. (i) PL spectra based on a single nanowire with a length of 10 μm excited at different energies at room temperature. (j) Multimode laser spectra of the selected DP-DHAQ microplate when excited by a pulsed laser (532 nm). Inset: fluorescence microscopy image of the selected microplate above the lasing threshold. [(b1), (b2) Reproduced with permission,[163] © 2015 WILEY-VCH. (c), (d) Reproduced with permission,[164] © 2016 WILEY-VCH. (f) Reproduced with permission,[169] © 2021 WILEY-VCH. (g)–(i) Reproduced with permission,[168] © 2020 Elsevier Inc. (j) Reproduced with permission,[171] © 2022 WILEY-VCH.]

6 NIR Organic Optical Waveguide

With the discovery of lasers, optical waveguides have attracted much interest from researchers because they offer another level of light control for various applications.[175] Organic optical waveguide materials have attracted much attention due to their low optical loss, structural diversity, and high refractive index compared to inorganic silicon-based optical waveguides.[176] Among them, the development of organic optical waveguide materials in the NIR region makes them a key area of interest in organic optical waveguide materials research because the three optical communication operating windows (850, 1310, and 1550 nm) with low loss rates are located in the NIR region. In this section, depending on the wavelength of the optical waveguide signals, we briefly introduce several representative single-component and multicomponent NIR organic optical waveguide materials.

An organometallic halide hybridized micro/nanorod with an NIR optical waveguide was reported by Yan et al.[177] The micro/nanorods were obtained based on the preparation of Pb-Bpeb (compound 78), where the structure of Pb-Bpeb and the SEM images of the micro/nanorods are shown in Fig. 10(a). Pb-Bpeb was obtained at with 1,4-bis[2-(4-pyridyl)-ethenyl] benzene (Bpeb) as the organic part, combined with the metal halide Pb. As shown in the PL image in Fig. 9(b), the Pb-Bpeb-based micro/nanorods were observed to have optical waveguiding phenomena at ~700 nm with a low α value of ~9.08 dB mm^{-1} [Fig. 9(c)], thus allowing them to avoid reabsorption of propagating light. This work provided a simple method for synthesizing a one-dimensional organic metal halide hybrid with excitation-dependent optical waveguide characteristics. In 2022, Liao et al. successfully prepared the first multilevel dendritic organic microwire crystals based on the organic NIR-emitting material DHNBP (compound 79) using a simple solution self-assembly method, which allowed the optical waveguide signal to be redshifted toward the communication window.[179] The molecular structure and the schematic diagram of multilevel dendritic organic micrometer wire crystals are

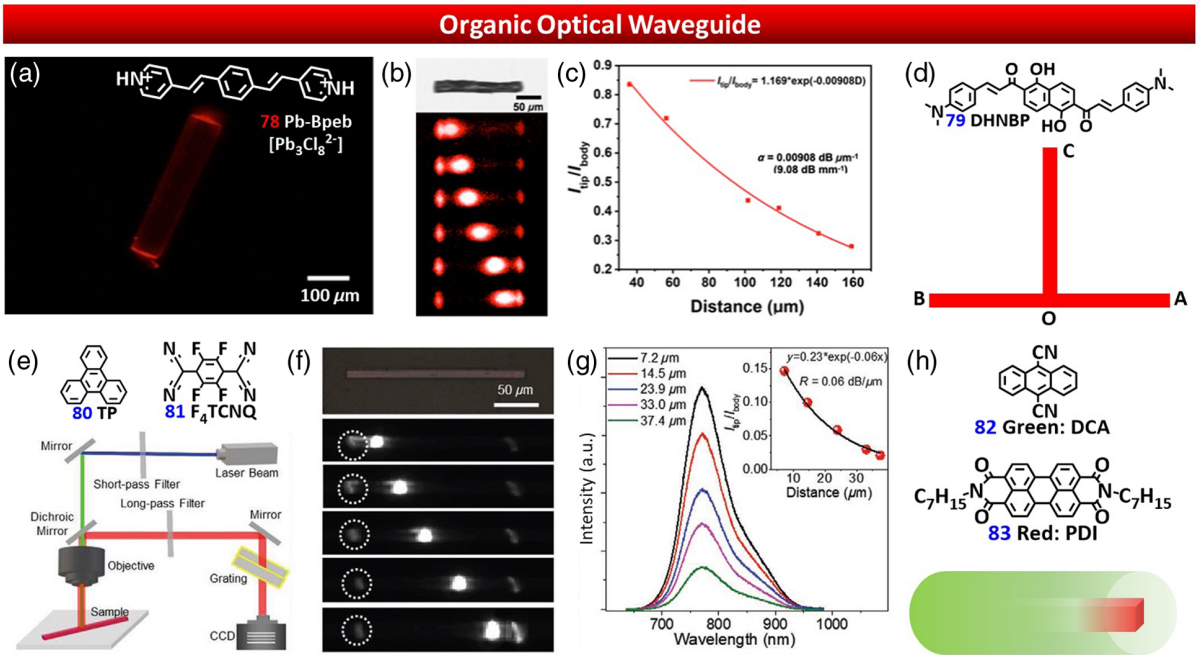

Fig. 10 (a) Fluorescence microscopy images of Pb-Bpeb. Inset: molecular structure of Pb-Bpeb. (b) 1D crystal by exciting the individual crystals at different positions with a laser beam ($\lambda = 405$ nm). (c) Intensity ratio I_{tip}/I_{body} against the distance. (d) Molecular structure of DHNBP and the diagram of the primary branched microwire. (e) Schematic illustration of the experimental setup used for optical waveguide measurement. (f) FM images obtained from an individual TP-F_4TCNQ microwire by excitation with a laser beam ($\lambda = 375$ nm) at different positions with a scale bar of 50 μm. (g) Corresponding spatially resolved PL spectra in (f) with different separation distances. Inset: ratios of the intensity I_{tip}/I_{body} against the distance d. (h) Molecular structure of DCA and DPI, schematic representation of the waveguide with relative dimensions, and the procedure for manual loading with PDI crystals. [(a)–(c) Reproduced with permission,[177] © 2021 ACS. (e)–(g) Reproduced with permission,[178] © 2022 WILEY-VCH.]

shown in Fig. 10(d). The lattice mismatch between the (100) and (010) crystal planes was as low as 5.3%, allowing the formation of multilevel branched microwires. Due to the unidirectional arrangement pattern of the molecules in the crystal, the multilevel dendritic micrometer lines had excellent optical properties. They excited the O position of the structure with a 375 nm laser beam and collected the external coupling emission spectra at tip positions A, B, and C. Interestingly, resonance peaks were evident in all spectra. For both the A and B position spectra, the $\Delta\lambda$ value was 2.4 nm, while the $\Delta\lambda$ value for the C position was 4.8 nm at a wavelength of 730 nm. This indicated that the backbone and branches could be FP-type resonators with little mutual interference between them.

By combining two or more crystalline materials with different but complementary optical properties, the resulting crystals can have the properties of multiple materials at the same time, thereby improving their performance and expanding their application range.[180] For example, Liao et al. prepared a CT cocrystal with NIR emission using triphenyl (TP, compound 80) as the donor and 2,3,5,6-tetrafluoro-7,7,8,8-tetracyanoquinoline dimethylmethane (F_4TCNQ, compound 81) as the acceptor.[178] The separated stacking mode of the TP-F_4TCNQ-CT complex had a low CT degree of 0.00103 and a small antipitch angle of 40 deg between the F_4TCNQ and TP molecules, which facilitated the realization of partial electron leap in the CT state to obtain attractive NIR emission. The TP-F_4TCNQ microwire with a length of 81.5 μm was tested as an optical waveguide [Fig. 10(g)] by a homemade microregion-based PL spectrometer [Fig. 10(f)]. As shown in Fig. 10(h), the corresponding PL signal collected at the tip with a peak of 770 nm showed a decrease in intensity with enhanced photon propagation distance (d) and exhibited an ultralow optical loss factor of 0.060 dB μm^{-1}. This work provided new insights into the exploration of new NIR-emitting organic materials through a "cocrystal" strategy. Naumov and coauthors extended the spectral range of organic crystal waveguides by using 9,10-dicyanoanthracene (DCA, compound 82) as a hollow crystal filled with crystals of its complementary perylene diimide derivative (PDI, compound 83); the structure of the prepared hybrid crystalline material is shown in Fig. 10(e).[181] The hybrid crystal could be used in both active and passive optical waveguides at 850 nm. Among other things, it had NIR emission when used in passive optical waveguides, indicating that the strategy successfully transmits light into the infrared region. This indicated that the report provided a new approach for developing smart optical waveguides based on organic molecular materials.

7 Conclusion and Outlook

In summary, we have reviewed representative NIR organic optoelectronic materials for OSCs, OPVs, OLEDs, organic lasers, and organic optical waveguides. We provided a brief overview of representative donors and acceptors in NIR OSCs, small molecule and polymer materials in NIR OPVs, representative materials in three generations of NIR OLEDs, dye-doped organic NIR lasers and NIR solid-state organic lasers, and the development of NIR organic optical waveguides. In addition, recent progress in device performances and properties was also briefly described. Although NIR organic optoelectronic materials have been developed rapidly in recent decades, as shown in Fig. 11, there are still some difficulties and challenges.

(1) There is still much room for material engineering. Although a number of NIR organic optoelectronic materials have been reported and applied in OSCs, OPDs, OLEDs, and other devices, organic NIR optoelectronic materials are still rare compared with these materials and devices in the visible light range. It is particularly important to develop high-performance organic NIR optoelectronic materials with high quantum yields, long wavelength absorption or emission, and good photoelectric response in order to increase the number of materials available for the fabrication of high-performance devices. Several methods have been proposed to design organic NIR photovoltaic materials. First, longer wavelength absorption and emission can be obtained by enlarging the π-conjugated system to reduce the HOMO-LUMO energy level gap or by modulating the D-A structure to enhance the ICT effect.[29,182] Second, the recombination energy can be allocated by increasing the delocalization length of excitons, thereby improving the quantum yield of the material.[183] In addition, the photoelectric response of the material can be improved by introducing polar functional groups into the material.[182] Many devices based on D-A structures have been reported in recent years. However, in-depth studies of the intramolecular and intermolecular interactions of these complex structures are still lacking. And there are still no effective methods to solve the common problems in devices such as dark current noise and high dark current density.

In order to effectively design high-performance materials and devices, simulation calculations involving DFT and molecular dynamics simulations may play an important role. For example, DFT can be used to calculate the relative energies of the ground state and excited state of a material to predict its optoelectronic properties and provide guidance for material design to obtain high performance. In addition, through molecular dynamics simulation, the growth direction of crystalline materials, crystal surface energy, intermolecular interactions, and changes in molecular morphology can be predicted, which can guide researchers to adjust the structure of the material to improve the performance. Actually, DFT calculation and molecular dynamics simulations have been widely used in the study of new material. For example, DFT calculation can be used to study the distribution of HOMO and LUMO orbitals. In the study of TADF materials, DFT calculations are often used to predict the TADF property from ΔE_{ST}.

Along with the development of artificial intelligence, machine learning has been widely studied in the assistance of medicine and materials design.[184–188] However, in the field of organic optoelectronic materials and devices, machine learning has not been well investigated. Therefore, artificial-intelligence-assisted design using density functional theory and molecular dynamics, etc., will be of great significance in order to effectively design high-performance materials and devices, and may generate new rules to guide future research on NIR organic materials and devices, resulting in new breakthroughs.

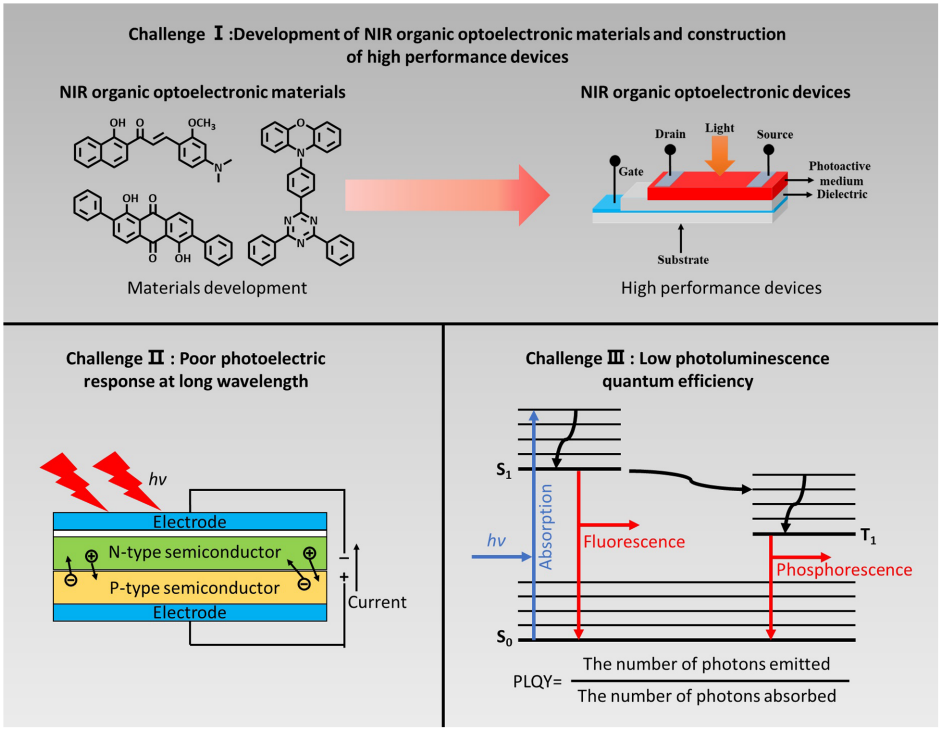

Fig. 11 Present challenges in organic NIR optoelectronic materials.

(2) For organic NIR-absorbing materials, although many materials with NIR absorption have been reported, most of them have poor optoelectronic responses at long wavelengths, making the device PCE less than a few percent. The low PCE is due to the weak absorption in the NIR range of the material and is often limited by the strong nonradiative transitions caused by the energy gap law. In addition, the deep HOMO and LUMO energy levels of narrow bandgap materials do not provide sufficient charge dissociation driving force, which also leads to a low PCE. Therefore, it is still necessary to develop organic NIR absorber materials with good optoelectronic responses at long wavelengths, thus enabling devices to obtain the desired PCE. Good photoelectric response can be achieved through the following strategies. First, modification of the D and A units may lead to changes in the energy levels and bandgaps and thus realize the possibility of obtaining organic NIR absorbing materials with good optoelectronic response. Second, side-chain engineering such as adjusting the substituent position and side-chain type also offers the possibility of achieving good optoelectronic response. In addition, the introduction of heteroatoms or the addition of dopants as well as the intercombination of different strategies may also achieve a good optoelectronic response at long wavelengths.

(3) For NIR organic light-emitting materials, due to the inherent fast nonradiative decay of narrow bandgap molecules, the PLQY of the materials is low, which hinders their development and application. Therefore, it is particularly important to improve the PLQY of NIR organic luminescence materials. The PLQY can be improved by modulating the morphology and crystalline phase of the molecule. Furthermore, we also demonstrated that PLQY can also be improved by introducing resonance-assisted intramolecular hydrogen bonding.[171]

In addition, devices based on NIR-emitting materials have a lower EQE at long wavelengths. Several methods have been used to improve the EQE of the devices. For example, the use of highly rigid donor or acceptor units in the material can be obtained to maximize the radiative excursion process and narrow the emission spectrum, which results in an increased EQE. In addition, our group recently proposed the method of distributing the complex energy by increasing the exciton off-domain length, which allows the material to overcome the energy gap law, resulting in an increase in the EQE of the device.[183]

Furthermore, gain materials are very important for lasers to achieve high performance. An effective energy level system can be constructed by utilizing dynamic chemical processes such as ESIPT to achieve effective population inversion to obtain better laser performance.[159] Organic crystal materials also have great potential for the preparation of high-performance lasers because they can be used as both a gain medium and an optical resonant cavity.[168,169]

In the future, the development trend of organic NIR optoelectronic materials may be toward the combination and common development of NIR absorption and emission materials. For example, very recently, Burke et al. achieved an NIR-II OLED with a D-A-D type material that was often used as an acceptor material in OSCs as the luminescent layer.[187] Second, the range of applications can be extended by integrating NIR absorbing and emitting materials. For example, by integrating NIR OPDs and OLEDs, So et al. enabled the device to realize both NIR detection and direct vision imaging.[189] In addition, NIR lasers with high monochromaticity can be combined with optical waveguides to realize optical waveguides at specific wavelengths to reduce optical loss, which has a large potential for application in the field of communications. Moreover, the development of NIR emitting materials and NIR detection materials can promote each other mutually. NIR detection materials have significant application value in medicine, agriculture, and scientific research due to their strong tissue penetration ability, fast detection speed, and the ability to qualitatively analyze samples. In order to promote the development of NIR detection technology, it is necessary to design and research high-performance NIR-emitting materials so as to promote the development of NIR-emitting materials.

In summary, although challenges exist, the future of organic NIR optoelectronic materials and devices is still full of possibility. We believe that, as these challenges are gradually overcome, significant advances in this field will be achieved in the near future.

Disclosures

The authors declare no conflicts of interest.

Code and Data Availability

Data underlying this study are available from the corresponding author upon reasonable request.

Acknowledgments

The authors acknowledge the financial support from the National Natural Science Foundation of China (Grant Nos. 52173177, 21971185, 22105139), the Natural Science Foundation of Jiangsu Province (Grant No. BK20221362), and the Science and Technology Support Program of Jiangsu Province (Grant No. TJ-2022-002). Furthermore, this work was supported by the Suzhou Key Laboratory of Functional Nano & Soft Materials, Collaborative Innovation Center of Suzhou Nano Science & Technology, the 111 Project, Joint International Research Laboratory of Carbon-Based Functional Materials and Devices, and Soochow University Tang Scholar.

References

1. J. Qi et al., "Advances in organic near-infrared materials and emerging applications," *Chem. Rec.* **16**(3), 1531–1548 (2016).
2. Y. Zhang et al., "Near-infrared emitting materials via harvesting triplet excitons: molecular design, properties, and application in organic light emitting diodes," *Adv. Opt. Mater.* **6**(18), 1800466 (2018).
3. L. Liu et al., "Er(3^+) sensitized 1530 nm to 1180 nm second near-infrared window upconversion nanocrystals for *in vivo* biosensing," *Angew. Chem. Int. Ed.* **57**(25), 7518–7522 (2018).
4. D. P. Karothu et al., "Mechanically robust amino acid crystals as fiber-optic transducers and wide bandpass filters for optical communication in the near-infrared," *Nat. Commun.* **12**(1), 1326 (2021).
5. B. Xie et al., "Near-infrared organic optoelectronic materials for light-harvesting systems: organic photovoltaics and organic photodiodes," *InfoMat* **2**(1), 57–91 (2019).
6. D. Meng et al., "Near-infrared materials: the turning point of organic photovoltaics," *Adv. Mater.* **34**(10), e2107330 (2022).
7. M. Zhang et al., "Highly stable nonhydroxyl antisolvent polymer dielectric: a new strategy towards high-performance low-temperature solution-processed ultraflexible organic transistors for skin-inspired electronics," *Research* **2021**, 9897353 (2021).
8. Z. L. Che et al., "Organic near-infrared luminescent materials based on excited state intramolecular proton transfer process," *Chin. J. Chem.* **40**(20), 2468–2481 (2022).

9. L. Dou et al., "Low-bandgap near-IR conjugated polymers/molecules for organic electronics," *Chem. Rev.* **115**(23), 12633–12665 (2015).
10. Z. Wu et al., "Emerging design and characterization guidelines for polymer-based infrared photodetectors," *Acc. Chem. Res.* **51**(12), 3144–3153 (2018).
11. Y. Hu et al., "Exciplex-based organic light-emitting diodes with near-infrared emission," *Adv. Optical Mater.* **8**(7), 1901917 (2020).
12. J. J. Wu et al., "Advances in near-infrared organic micro/nanolasers," *Adv. Optical Mater.* **11**, 2200815 (2022).
13. S. Chen et al., "Optical waveguides based on one-dimensional organic crystals," *PhotoniX* **2**(1), 2 (2021).
14. Y. Li et al., "Near-infrared ternary tandem solar cells," *Adv. Mater.* **30**(45), e1804416 (2018).
15. F. Liu et al., "Efficient semitransparent solar cells with high NIR responsiveness enabled by a small-bandgap electron acceptor," *Adv. Mater.* **29**(21), 1606574 (2017).
16. X. Liu et al., "Recent advances in organic near-infrared photodiodes," *J. Mater. Chem. C* **6**(14), 3499–3513 (2018).
17. H. Xu et al., "Flexible organic/inorganic hybrid near-infrared photoplethysmogram sensor for cardiovascular monitoring," *Adv. Mater.* **29**(31), 1700975 (2017).
18. Z. Tang et al., "Polymer:fullerene bimolecular crystals for near-infrared spectroscopic photodetectors," *Adv. Mater.* **29**(33), 1702184 (2017).
19. G. Simone et al., "Near-infrared tandem organic photodiodes for future application in artificial retinal implants," *Adv. Mater.* **30**(51), e1804678 (2018).
20. B. M. Savoie et al., "Mesoscopic features of charge generation in organic semiconductors," *Acc. Chem. Res.* **47**(11), 3385–3394 (2014).
21. S. D. Dimitrov and J. R. Durrant, "Materials design considerations for charge generation in organic solar cells," *Chem. Mater.* **26**(1), 616–630 (2013).
22. H. Xiang et al., "Near-infrared phosphorescence: materials and applications," *Chem. Soc. Rev.* **42**(14), 6128–6185 (2013).
23. X. Han et al., "Highly efficient solid-state near-infrared emitting material based on triphenylamine and diphenylfumaronitrile with an EQE of 2.58% in nondoped organic light-emitting diode," *Adv. Funct. Mater.* **25**(48), 7521–7529 (2015).
24. J. J. Wu et al., "Advances in energy-level systems of organic lasers," *Laser Photonics Rev.* **16**(12), 2200366 (2022).
25. J. Clark and G. Lanzani, "Organic photonics for communications," *Nat. Photonics* **4**(7), 438–446 (2010).
26. B. Mizaikoff, "Waveguide-enhanced mid-infrared chem/bio sensors," *Chem. Soc. Rev.* **42**(22), 8683–8699 (2013).
27. X. Yu et al., "Deep-red-emissive flexible optical waveguide with high elastic performance based on an organic crystal," *ChemPhotoChem* **6**(6), e202200038 (2022).
28. Y. S. Zhao et al., "Patterned growth of vertically aligned organic nanowire waveguide arrays," *ACS Nano* **4**(3), 1630–1636 (2010).
29. J. Zhang et al., "Recent progress in near-infrared organic electroluminescent materials," *Top. Curr. Chem.* **380**(1), 6 (2021).
30. M. A. Baldo et al., "Highly efficient phosphorescent emission from organic electroluminescent devices," *Nature* **395**(6698), 151 (1998).
31. D. H. Lim et al., "Recent progress of ultra-narrow-bandgap polymer donors for NIR-absorbing organic solar cells," *Nanosc. Adv.* **3**(15), 4306 (2021).
32. N. Li et al., "Advances in solution-processable near-infrared phototransistors," *J. Mater. Chem. C* **7**(13), 3711–3729 (2019).
33. Q. Li et al., "Exploration of near-infrared organic photodetectors," *Chem. Mater.* **31**(17), 6359–6379 (2019).
34. A. Zampetti et al., "Near-infrared (NIR) organic light-emitting diodes (OLEDs): challenges and opportunities," *Adv. Funct. Mater.* **29**(21), 1807623 (2019).
35. Y. Zhang and J. Qiao, "Near-infrared emitting iridium complexes: molecular design, photophysical properties, and related applications," *iScience* **24**(8), 102858 (2021).
36. J. X. Chen et al., "Red/near-infrared thermally activated delayed fluorescence OLEDs with near 100% internal quantum efficiency," *Angew. Chem. Int. Ed.* **58**(41), 14660–14665 (2019).
37. J.-J. Wu et al., "Near-infrared solid-state lasers based on small organic molecules," *ACS Photonics* **6**(11), 2590–2599 (2019).
38. Y. J. Yu et al., "Harvesting triplet excitons for near-infrared electroluminescence via thermally activated delayed fluorescence channel," *iScience* **24**(2), 102123 (2021).
39. G. P. Kini et al., "Latest progress on photoabsorbent materials for multifunctional semitransparent organic solar cells," *Adv. Funct. Mater.* **31**(15), 2007931 (2021).
40. K. Gao et al., "Low-bandgap porphyrins for highly efficient organic solar cells: materials, morphology, and applications," *Adv. Mater.* **32**(32), e1906129 (2020).
41. P. Cheng et al., "Next-generation organic photovoltaics based on non-fullerene acceptors," *Nat. Photonics* **12**(3), 131–142 (2018).
42. C. Yan et al., "Non-fullerene acceptors for organic solar cells," *Nat. Rev. Mater.* **3**(3), 18003 (2018).
43. Q. Xue et al., "Recent advances in semi-transparent polymer and perovskite solar cells for power generating window applications," *Energy Environ. Sci.* **11**(7), 1688–1709 (2018).
44. J. Qin et al., "Recent progress in flexible and stretchable organic solar cells," *Adv. Funct. Mater.* **30**(36), 2002529 (2020).
45. H. Sun et al., "Recent progress on non-fullerene acceptors for organic photovoltaics," *Mater. Today* **24**, 94–118 (2019).
46. C. J. Brabec et al., "Influence of blend microstructure on bulk heterojunction organic photovoltaic performance," *Chem. Soc. Rev.* **40**(3), 1185–1199 (2011).
47. G. Li et al., "Polymer solar cells," *Nat. Photonics* **6**(3), 153–161 (2012).
48. W. Gao et al., "Near-infrared absorbing nonfullerene acceptors for organic solar cells," *Sol. RRL* **6**(1), 2100868 (2021).
49. J. Zhang et al., "Material insights and challenges for non-fullerene organic solar cells based on small molecular acceptors," *Nat. Energy* **3**(9), 720–731 (2018).
50. J. H. Hou et al., "Synthesis, characterization, and photovoltaic properties of a low band gap polymer based on silole-containing polythiophenes and 2,1,3-benzothiadiazole," *J. Am. Chem. Soc.* **130**(48), 16144–16145 (2008).
51. M. M. Wienk et al., "Narrow-bandgap diketo-pyrrolo-pyrrole polymer solar cells: the effect of processing on the performance," *Adv. Mater.* **20**(13), 2556–2560 (2008).
52. P. Zhou et al., "Thiophene-fused benzothiadiazole: a strong electron-acceptor unit to build D–A copolymer for highly efficient polymer solar cells," *Chem. Mater.* **26**(11), 3495–3501 (2014).
53. W. Chen and Q. Zhang, "Recent progress in non-fullerene small molecule acceptors in organic solar cells (OSCs)," *J. Mater. Chem. C* **6**(6), 1275–1302 (2017).
54. S. Dai and X. Zhan, "Nonfullerene acceptors for semitransparent organic solar cells," *Adv. Energy Mater.* **8**(21), 1800002 (2018).
55. X. Fan et al., "Ladder-type nonacyclic arene bis(thieno[3,2-b]thieno)cyclopentafluorene as a promising building block for non-fullerene acceptors," *Chem. Asian J.* **14**(10), 1814–1822 (2019).
56. W. Liu et al., "Low-bandgap non-fullerene acceptors enabling high-performance organic solar cells," *ACS Energy Lett.* **6**(2), 598–608 (2021).
57. H. Sun et al., "PDI derivative through fine-tuning the molecular structure for fullerene-free organic solar cells," *ACS Appl. Mater. Interfaces* **9**(35), 29924–29931 (2017).
58. H.-Y. Chen et al., "Polymer solar cells with enhanced open-circuit voltage and efficiency," *Nat. Photonics* **3**(11), 649–653 (2009).
59. S. H. Liao et al., "Fullerene derivative-doped zinc oxide nanofilm as the cathode of inverted polymer solar cells with low-bandgap

polymer (PTB7-Th) for high performance," *Adv. Mater.* **25**(34), 4766–4771 (2013).
60. Y. Zhao et al., "Diketopyrrolopyrrole based A2-D-A1-D-A2 type small molecules for organic solar cells: effects of substitution of benzene with thiophene," *Dyes Pigm.* **130**, 282–290 (2016).
61. J. C. Bijleveld et al., "Poly(diketopyrrolopyrrole-terthiophene) for ambipolar logic and photovoltaics," *J. Am. Chem. Soc.* **131**(46), 16616–16617 (2009).
62. G. Oklem et al., "A new NIR absorbing DPP-based polymer for thick organic solar cells," *J. Mater. Chem. C* **6**(12), 2957–2961 (2018).
63. B. Hu et al., "Novel donor–acceptor polymers based on 7-perfluorophenyl-6H-[1,2,5]thiadiazole[3,4-g]benzoimidazole for bulk heterojunction solar cells," *RSC Adv.* **6**(62), 50137–50145 (2015).
64. D. Mühlbacher et al., "High photovoltaic performance of a low-bandgap polymer," *Adv. Mater.* **18**(21), 2884–2889 (2006).
65. J. You et al., "A polymer tandem solar cell with 10.6% power conversion efficiency," *Nat. Commun.* **4**(1), 1446 (2013).
66. S. Chen et al., "A visible-near-infrared absorbing A–π2–D–π1–D–π2–A type dimeric-porphyrin donor for high-performance organic solar cells," *J. Mater. Chem. A* **6**(48), 25460–25468 (2017).
67. F. Yang et al., "A simple, small-bandgap porphyrin-based conjugated polymer for application in organic electronics," *Macromol. Rapid Commun.* **39**(21), e1800546 (2018).
68. P. Cheng and Y. Yang, "Narrowing the band gap: the key to high-performance organic photovoltaics," *Acc. Chem. Res.* **53**(6), 1218–1228 (2020).
69. C. Y. Yu et al., "Thiophene/phenylene/thiophene-based low-bandgap conjugated polymers for efficient near-infrared photovoltaic applications," *Chem. Mater.* **21**(14), 3262–3269 (2009).
70. W. Li et al., "Diketopyrrolopyrrole polymers for organic solar cells," *Acc. Chem. Res.* **49**(1), 78–85 (2016).
71. W. Chen et al., "Synthesis and photovoltaic properties of novel C_{60} bisadducts based on benzo[2,1,3]-thiadiazole," *Tetrahedron* **70**(36), 6217–6221 (2014).
72. J. Zhang et al., "Highly efficient semitransparent organic solar cells with color rendering index approaching 100," *Adv. Mater.* **31**(10), e1807159 (2019).
73. Y. Lin et al., "An electron acceptor challenging fullerenes for efficient polymer solar cells," *Adv. Mater.* **27**(7), 1170–1174 (2015).
74. P. Cheng et al., "Transparent hole-transporting frameworks: a unique strategy to design high-performance semitransparent organic photovoltaics," *Adv. Mater.* **32**(39), e2003891 (2020).
75. X. Zhang et al., "Dithienopyrrole-based donor–acceptor copolymers: low band-gap materials for charge transport, photovoltaics and electrochromism," *J. Mater. Chem.* **20**(1), 123–134 (2010).
76. M. L. Keshtov et al., "Synthesis and characterization of a low band gap quinoxaline based D–A copolymer and its application as a donor for bulk heterojunction polymer solar cells," *Polym. Chem.* **4**(14), 4033–4044 (2013).
77. V. Tamilavan et al., "Synthesis of new near infrared absorption polymers based on thiadiazoloquinoxaline and their solar cell applications," *Synth. Met.* **162**, 1184–1189 (2012).
78. D. G. Farnum et al., "Attempted reformatskii reaction of benzonitrile, 1,4-diketo-3,6-diphenylpyrrolo[3,4-c]pyrrole. A – lactam analog of pentalene," *Tetrahedron Lett.* **15**(29), 2549–2552 (1974).
79. L. J. Huo et al., "Bandgap and molecular level control of the low-bandgap polymers based on 3,6-dithiophen-2-yl-2,5-dihydropyrrolo 3,4-c pyrrole-1,4-dione toward highly efficient polymer solar cells," *Macromolecules* **42**(17), 6564–6571 (2009).
80. J. Hou et al., "Organic solar cells based on non-fullerene acceptors," *Nat. Mater.* **17**(2), 119–128 (2018).
81. Q. Yue et al., "N-type molecular photovoltaic materials: design strategies and device applications," *J. Am. Chem. Soc.* **142**(27), 11613–11628 (2020).
82. G. Zhang et al., "Nonfullerene acceptor molecules for bulk heterojunction organic solar cells," *Chem. Rev.* **118**(7), 3447–3507 (2018).
83. C. B. Nielsen et al., "Non-fullerene electron acceptors for use in organic solar cells," *Acc. Chem. Res.* **48**(11), 2803–2812 (2015).
84. J. Wang and X. Zhan, "Fused-ring electron acceptors for photovoltaics and beyond," *Acc. Chem. Res.* **54**(1), 132–143 (2021).
85. B. Kan et al., "Small-molecule acceptor based on the heptacyclic benzodi(cyclopentadithiophene) unit for highly efficient non-fullerene organic solar cells," *J. Am. Chem. Soc.* **139**(13), 4929–4934 (2017).
86. H. Wang et al., "Nonacyclic carbazole-based non-fullerene acceptors enable over 12% efficiency with enhanced stability for organic solar cells," *J. Mater. Chem. A* **7**(38), 21903–21910 (2019).
87. Z. G. Zhang et al., "Constructing a strongly absorbing low-bandgap polymer acceptor for high-performance all-polymer solar cells," *Angew. Chem. Int. Ed.* **56**(43), 13503–13507 (2017).
88. J. Sun et al., "Dithieno[3,2-b:2′,3′-d]pyrrol fused nonfullerene acceptors enabling over 13% efficiency for organic solar cells," *Adv. Mater.* **30**(16), e1707150 (2018).
89. J. Yuan et al., "Single-junction organic solar cell with over 15% efficiency using fused-ring acceptor with electron-deficient core," *Joule* **3**(4), 1140–1151 (2019).
90. Z. Jia et al., "High performance tandem organic solar cells via a strongly infrared-absorbing narrow bandgap acceptor," *Nat. Commun.* **12**(1), 178 (2021).
91. J. Yuan et al., "Enabling low voltage losses and high photocurrent in fullerene-free organic photovoltaics," *Nat. Commun.* **10**(1), 570 (2019).
92. D. Yang and D. Ma, "Development of organic semiconductor photodetectors: from mechanism to applications," *Adv. Optical Mater.* **7**(1), 1800522 (2019).
93. G. Qian and Z. Y. Wang, "Near-infrared organic compounds and emerging applications," *Chem. Asian J.* **6**(5), 1006–1029 (2010).
94. G. Qian et al., "Family of diazapentalene chromophores and narrow-band-gap polymers: synthesis, halochromism, halofluorism, and visible–near infrared photodetectivity," *Chem. Mater.* **24**(12), 2364–2372 (2012).
95. E. Perzon et al., "A conjugated polymer for near infrared optoelectronic applications," *Adv. Mater.* **19**(20), 3308–3311 (2007).
96. Z. Su et al., "High-performance organic small-molecule panchromatic photodetectors," *ACS Appl. Mater. Interfaces* **7**(4), 2529–2534 (2015).
97. M. Zhu et al., "Enhanced near-infrared photoresponse of organic phototransistors based on single-component donor-acceptor conjugated polymer nanowires," *Nanoscale* **8**(14), 7738–7748 (2016).
98. Y. Yao et al., "Plastic near-infrared photodetectors utilizing low band gap polymer," *Adv. Mater.* **19**(22), 3979–3983 (2007).
99. M. Wang et al., "High open circuit voltage in regioregular narrow band gap polymer solar cells," *J. Am. Chem. Soc.* **136**(36), 12576–12579 (2014).
100. S. Park et al., "Ultraflexible near-infrared organic photodetectors for conformal photoplethysmogram sensors," *Adv. Mater.* **30**(34), e1802359 (2018).
101. X. Gong et al., "High-detectivity polymer photodetectors with spectral response from 300 nm to 1450 nm," *Science* **325**(5948), 1665–1667 (2009).
102. M. Li et al., "Phenanthrene condensed thiadiazoloquinoxaline donor–acceptor polymer for phototransistor applications," *Chem. Mater.* **27**(6), 2218–2223 (2015).

103. L. Zheng et al., "Solution-processed broadband polymer photodetectors with a spectral response of up to 2.5 μm by a low bandgap donor–acceptor conjugated copolymer," *J. Mater. Chem. C* **6**(14), 3634–3641 (2018).
104. Q. X. Tang et al., "Photoswitches and phototransistors from organic single-crystalline submicro/nanometer ribbons," *Adv. Mater.* **19**(18), 2624–2628 (2007).
105. L. Li et al., "Highly responsive organic near-infrared photodetectors based on a porphyrin small molecule," *J. Mater. Chem. C* **2**(8), 1372–1375 (2014).
106. C. Wang et al., "N-type 2D organic single crystals for high-performance organic field-effect transistors and near-infrared phototransistors," *Adv. Mater.* **30**(16), e1706260 (2018).
107. J. Huang et al., "A high-performance solution-processed organic photodetector for near-infrared sensing," *Adv. Mater.* **32**(1), e1906027 (2020).
108. S. Deng et al., "A simple fused-ring acceptor toward high-sensitivity binary near-infrared photodetector," *Adv. Optical Mater.* **10**(12), 2200371 (2022).
109. M. Young et al., "Organic heptamethine salts for photovoltaics and detectors with near-infrared photoresponse up to 1600 nm," *Adv. Optical Mater.* **4**(7), 1028–1033 (2016).
110. Y. Lin et al., "A solution-processable small molecule based on benzodithiophene and diketopyrrolopyrrole for high-performance organic solar cells," *Adv. Energy Mater.* **3**(9), 1166–1170 (2013).
111. M. T. Lloyd et al., "Photovoltaics from soluble small molecules," *Mater. Today* **10**(11), 34–41 (2007).
112. B. Walker et al., "Nanoscale phase separation and high photovoltaic efficiency in solution-processed, small-molecule bulk heterojunction solar cells," *Adv. Funct. Mater.* **19**(19), 3063–3069 (2009).
113. Z. Wu et al., "The role of dielectric screening in organic shortwave infrared photodiodes for spectroscopic image sensing," *Adv. Funct. Mater.* **28**(50), 1805738 (2018).
114. A. N. Bashkatov et al., "Optical properties of human skin, subcutaneous and mucous tissues in the wavelength range from 400 to 2000 nm," *J. Phys. D: Appl. Phys.* **38**(15), 2543–2555 (2005).
115. V. C. Bender et al., "Solid-state lighting: a concise review of the state of the art on LED and OLED modeling," *IEEE Ind. Electron. Mag.* **9**(2), 6–16 (2015).
116. M. Ibrahim-Ouali and F. Dumur, "Recent advances on metal-based near-infrared and infrared emitting OLEDs," *Molecules* **24**(7), 1412 (2019).
117. Y. Yu et al., "Solution-processed AIEgen NIR OLEDs with EQE approaching 15%," *Angew. Chem. Int. Ed.* **61**(26), e202204279 (2022).
118. S. T. Le et al., "10 Mb/s visible light transmission system using a polymer light-emitting diode with orthogonal frequency division multiplexing," *Opt. Lett.* **39**(13), 3876–3879 (2014).
119. P. A. Haigh et al., "Visible light communications: real time 10 Mb/s link with a low bandwidth polymer light-emitting diode," *Opt. Express* **22**(3), 2830–2838 (2014).
120. F. Liu et al., "High-efficiency near-infrared fluorescent organic light-emitting diodes with small efficiency roll-off based on AIE-active phenanthro[9,10-d]imidazole derivatives," *J. Mater. Chem. C* **8**(20), 6883–6890 (2020).
121. G. Qian et al., "Simple and efficient near-infrared organic chromophores for light-emitting diodes with single electroluminescent emission above 1000 nm," *Adv. Mater.* **21**(1), 111–116 (2009).
122. X. Du et al., "Efficient non-doped near infrared organic light-emitting devices based on fluorophores with aggregation-induced emission enhancement," *Chem. Mater.* **24**(11), 2178–2185 (2012).
123. G. Tregnago et al., "Thia- and selena-diazole containing polymers for near-infrared light-emitting diodes," *J. Mater. Chem. C* **3**(12), 2792–2797 (2015).
124. C.-L. Ho et al., "Red to near-infrared organometallic phosphorescent dyes for OLED applications," *J. Organomet. Chem.* **751**, 261 (2014).
125. C. Adachi et al., "Nearly 100% internal phosphorescence efficiency in an organic light-emitting device," *J. Appl. Phys.* **90**(10), 5048–5051 (2001).
126. M. A. Baldo et al., "Very high-efficiency green organic light-emitting devices based on electrophosphorescence," *Appl. Phys. Lett.* **75**(1), 4–6 (1999).
127. W. P. Gillin and R. J. Curry, "Erbium (III) tris(8-hydroxyquinoline) (ErQ): a potential material for silicon compatible 1.5 μm emitters," *Appl. Phys. Lett.* **74**(6), 798–799 (1999).
128. R. J. Curry and W. P. Gillin, "1.54 μm electroluminescence from erbium (III) tris(8-hydroxyquinoline) (ErQ)-based organic light-emitting diodes," *Appl. Phys. Lett.* **75**(10), 1380–1382 (1999).
129. E. L. Williams et al., "Organic light-emitting diodes having exclusive near-infrared electrophosphorescence," *Appl. Phys. Lett.* **89**(8), 083506 (2006).
130. L. Huang et al., "Platinum (II) azatetrabenzoporphyrins for near-infrared organic light-emitting diodes," *Appl. Phys. Lett.* **109**(23), 233302 (2016).
131. K. Tuong Ly et al., "Near-infrared organic light-emitting diodes with very high external quantum efficiency and radiance," *Nat. Photonics* **11**(1), 63–68 (2016).
132. S.-F. Wang et al., "Polyatomic molecules with emission quantum yields >20% enable efficient organic light-emitting diodes in the NIR(II) window," *Nat. Photonics* **16**(12), 843–850 (2022).
133. D. Volz et al., "From iridium and platinum to copper and carbon: new avenues for more sustainability in organic light-emitting diodes," *Green Chem.* **17**(4), 1988–2011 (2015).
134. F. B. Dias et al., "Photophysics of thermally activated delayed fluorescence molecules," *Methods Appl. Fluoresc.* **6**(1), 012001 (2017).
135. T. J. Penfold, "On predicting the excited-state properties of thermally activated delayed fluorescence emitters," *J. Phys. Chem. C* **119**(24), 13535–13544 (2015).
136. W. Zeng et al., "Achieving nearly 30% external quantum efficiency for orange-red organic light-emitting diodes by employing thermally activated delayed fluorescence emitters composed of 1,8-naphthalimide-acridine hybrids," *Adv. Mater.* **30**(5), 1704961 (2018).
137. D. R. Lee et al., "Above 30% external quantum efficiency in green delayed fluorescent organic light-emitting diodes," *ACS Appl. Mater. Interfaces* **7**(18), 9625–9629 (2015).
138. M. Kim et al., "Stable blue thermally activated delayed fluorescent organic light-emitting diodes with three times longer lifetime than phosphorescent organic light-emitting diodes," *Adv. Mater.* **27**(15), 2515–2520 (2015).
139. S. Wang et al., "Highly efficient near-infrared delayed fluorescence organic light-emitting diodes using a phenanthrene-based charge-transfer compound," *Angew. Chem. Int. Ed.* **54**(44), 13068–13072 (2015).
140. C. Li et al., "Deep-red to near-infrared thermally activated delayed fluorescence in organic solid films and electroluminescent devices," *Angew. Chem. Int. Ed.* **56**(38), 11525–11529 (2017).
141. Y. Yuan et al., "Over 10% EQE near-infrared electroluminescence based on a thermally activated delayed fluorescence emitter," *Adv. Funct. Mater.* **27**(26), 1700986 (2017).
142. R. Nagata et al., "Near-infrared electrophosphorescence up to 1.1 μm using a thermally activated delayed fluorescence molecule as triplet sensitizer," *Adv. Mater.* **29**(5), 1604265 (2017).
143. U. Balijapalli et al., "Highly efficient near-infrared electrofluorescence from a thermally activated delayed fluorescence molecule," *Angew. Chem. Int. Ed.* **60**(15), 8477–8482 (2021).
144. T. H. Maiman, "Stimulated optical radiation in ruby," *Nature* **187**(4736), 493–494 (1960).
145. Y. C. Chen and X. Fan, "Biological lasers for biomedical applications," *Adv. Opt. Mater.* **7**(17), 1900377 (2019).

146. J. Liang et al., "Organic microlaser arrays: from materials engineering to optoelectronic applications," *Acc. Mater. Res.* **2**(5), 340–351 (2021).
147. C. Zhang et al., "Organic printed photonics: from microring lasers to integrated circuits," *Sci. Adv.* **1**(8), e1500257 (2015).
148. C.-C. Yan et al., "Organic lasers harnessing excited state intramolecular proton transfer process," *ACS Photonics* **7**(6), 1355–1366 (2020).
149. F. P. Schafer et al., "Organic dye solution laser," *Appl. Phys. Lett.* **9**(8), 306–309 (1966).
150. I. D. W. Samuel and G. A. Turnbull, "Organic semiconductor lasers," *Chem. Rev.* **107**(4), 1272–1295 (2007).
151. A. J. Kuehne and M. C. Gather, "Organic lasers: recent developments on materials, device geometries, and fabrication techniques," *Chem. Rev.* **116**(21), 12823–12864 (2016).
152. C. C. Yan et al., "Thermally activated delayed fluorescent gain materials: harvesting triplet excitons for lasing," *Adv. Sci.* **9**(16), e2200525 (2022).
153. Y.-Z. Ma et al., "Exciton–exciton annihilation in copper-phthalocyanine single-crystal nanowires," *J. Phys. Chem. C* **116**(40), 21588–21593 (2012).
154. T. Kobayashi et al., "Near-infrared laser emission from luminescent plastic waveguides," *Appl. Phys. Lett.* **85**(2), 185–187 (2004).
155. C. Zhang et al., "Two-photon pumped lasing in single-crystal organic nanowire exciton polariton resonators," *J. Am. Chem. Soc.* **133**(19), 7276–7279 (2011).
156. H.-H. Fang et al., "Functional organic single crystals for solid-state laser applications," *Laser Photonics Rev.* **8**(5), 687–715 (2014).
157. W. Zhang et al., "Organic micro/nanoscale lasers," *Acc. Chem. Res.* **49**(9), 1691–1700 (2016).
158. S. Yuyama et al., "Solid-state organic laser emission at 970 nm from dye-doped fluorinated-polyimide planar waveguides," *Appl. Phys. Lett.* **93**(2), 023306 (2008).
159. C. C. Yan et al., "Excited-state intramolecular proton transfer parent core engineering for six-level system lasing toward 900 nm," *Angew. Chem. Int.* **61**(48), e202210422 (2022).
160. D.-H. Kim et al., "High-efficiency electroluminescence and amplified spontaneous emission from a thermally activated delayed fluorescent near-infrared emitter," *Nat. Photonics* **12**(2), 98–104 (2018).
161. H. Ye et al., "Near-infrared electroluminescence and low threshold amplified spontaneous emission above 800 nm from a thermally activated delayed fluorescent emitter," *Chem. Mater.* **30**(19), 6702–6710 (2018).
162. Y. Liu et al., "Suppressing nonradiative processes of organic dye with metal-organic framework encapsulation toward near-infrared solid-state microlasers," *ACS Appl. Mater. Interfaces* **10**(41), 35455–35461 (2018).
163. X. Cheng et al., "Organic crystals with near-infrared amplified spontaneous emissions based on 2′-hydroxychalcone derivatives: subtle structure modification but great property change," *Angew. Chem. Int. Ed.* **54**(29), 8369–8373 (2015).
164. X. Cheng et al., "Multicolor amplified spontaneous emissions based on organic polymorphs that undergo excited-state intramolecular proton transfer," *Chem. Eur. J.* **22**(14), 4899–4903 (2016).
165. X. Wang et al., "Near-infrared lasing from small-molecule organic hemispheres," *J. Am. Chem. Soc.* **137**(29), 9289–9295 (2015).
166. X. Wang et al., "Tunable near-infrared organic nanowire nanolasers," *Adv. Funct. Mater.* **27**(45), 1703470 (2017).
167. X. Wang et al., "Near-infrared organic single-crystal lasers with polymorphism-dependent excited state intramolecular proton transfer," *Adv. Optical Mater.* **6**(12), 1700027 (2017).
168. J.-J. Wu et al., "Near-infrared organic single-crystal nanolaser arrays activated by excited-state intramolecular proton transfer," *Matter* **2**(5), 1233–1243 (2020).
169. J. J. Wu et al., "Cascaded excited-state intramolecular proton transfer towards near-infrared organic lasers beyond 850 nm," *Angew. Chem. Int. Ed.* **60**(16), 9114–9119 (2021).
170. B. Fang et al., "Near-infrared microlasers from self-assembled spiropyrane-based microspherical caps," *ACS Appl. Mater. Interfaces* **11**(41), 38226–38231 (2019).
171. W. Y. Yang et al., "Deepening insights into near-infrared excited-state intramolecular proton transfer lasing: the charm of resonance-assisted hydrogen bonds," *Adv. Funct. Mater.* **32**(39), 2204129 (2022).
172. S. M. Yoon et al., "Optical waveguiding and lasing action in porphyrin rectangular microtube with subwavelength wall thicknesses," *Acs Nano* **6**(4), 2923–2929 (2011).
173. C. Wei et al., "Excimer emission in self-assembled organic spherical microstructures: an effective approach to wavelength switchable microlasers," *Adv. Optical Mater.* **4**(7), 1009–1014 (2016).
174. J. Gierschner et al., "Organic single crystal lasers: a materials view," *Adv. Optical Mater.* **4**(3), 348–364 (2016).
175. F. Chen and J. R. V. de Aldana, "Optical waveguides in crystalline dielectric materials produced by femtosecond-laser micromachining," *Laser Photonics Rev.* **8**(2), 251–275 (2014).
176. D. Tian and Y. Chen, "Optical waveguides in organic crystals of polycyclic arenes," *Adv. Opt. Mater.* **9**(23), 2002264 (2021).
177. S. Wu et al., "Low-dimensional organic metal halide hybrids with excitation-dependent optical waveguides from visible to near-infrared emission," *ACS Appl. Mater. Interfaces* **13**(22), 26451–26460 (2021).
178. M. P. Zhuo et al., "Segregated array tailoring charge-transfer degree of organic cocrystal for the efficient near-infrared emission beyond 760 nm," *Adv. Mater.* **34**(11), e2107169 (2022).
179. C.-C. Yan et al., "Precise synthesis of multilevel branched organic microwires for optical signal processing in the near infrared region," *Sci. China Mater.* **65**(4), 1020–1027 (2021).
180. Y. Huang et al., "Organic cocrystals: beyond electrical conductivities and field-effect transistors (FETs)," *Angew. Chem. Int. Ed.* **58**(29), 9696–9711 (2019).
181. L. Catalano et al., "A filled organic crystal as a hybrid large-bandwidth optical waveguide," *Chem. Commun.* **55**(34), 4921–4924 (2019).
182. X. Huang et al., "Low-bandgap conjugated polymers with photocurrent response over 1000 nm," *J. Mater. Sci.* **56**(14), 8334 (2021).
183. Y.-C. Wei et al., "Overcoming the energy gap law in near-infrared OLEDs by exciton–vibration decoupling," *Nat. Photonics* **14**(9), 570–577 (2020).
184. H. Lu et al., "Machine learning-aided engineering of hydrolases for PET depolymerization," *Nature* **604**(7907), 662–667 (2022).
185. A. A. Sadybekov et al., "Synthon-based ligand discovery in virtual libraries of over 11 billion compounds," *Nature* **601**(7893), 452–459 (2022).
186. J. A. Hueffel et al., "Accelerated dinuclear palladium catalyst identification through unsupervised machine learning," *Science* **374**(6571), 1134–1140 (2021).
187. N. H. Angello et al., "Closed-loop optimization of general reaction conditions for heteroaryl Suzuki-Miyaura coupling," *Science* **378**(6618), 399–405 (2022).
188. B. Mikulak-Klucznik et al., "Computational planning of the synthesis of complex natural products," *Nature* **588**(7836), 83–88 (2020).
189. D. Y. Kim et al., "Multi-spectral imaging with infrared sensitive organic light emitting diode," *Sci. Rep.* **4**(1), 5946 (2014).

Zong-Lu Che received his bachelor's degree in polymer material and engineering from the University of Jinan in 2021. Now, he is pursuing his master's degree under the supervision of Prof. Liang-Sheng Liao and Prof. Xue-Dong Wang at the Institute of Functional Nano and Soft Materials (FUNSOM) of Soochow University. His current research

interests include the design and synthesis of organic luminescent materials and their application in organic solid-state lasers.

Chang-Cun Yan received his PhD from the College of Chemistry, Nankai University, in 2017. After completing his postdoctoral work at the Institute of Functional Nano and Soft Materials (FUNSOM), Soochow University, he joined the College of Chemistry, Chemical Engineering and Materials Science, Soochow University. His current research focuses on the design, synthesis, and application of organic semiconductor materials and organic photonics.

Xue-Dong Wang is a full professor at the Institute of Functional Nano and Soft Materials (FUNSOM) of Soochow University. He received his PhD in physical chemistry from the Institute of Chemistry, Chinese Academy of Sciences, in 2016. His research focuses on the fine synthesis of organic micro/nanocrystals and organic photonics, including organic solid-state lasers and optical waveguides.

Liang-Sheng Liao received his PhD in physics from Nanjing University, China. After working at Eastman Kodak Company as a senior research scientist from 2000 to 2009, he joined the Institute of Functional Nano and Soft Materials (FUNSOM), Soochow University, as a full professor. His current research interests include materials and architectures of OLEDs as well as organic lasers, quantum-dot LEDs, organic solar cells, and perovskite solar cells.